PNEUMATICALLY-POWERED ROBOTIC EXOSKELETON TO EXERCISE SPECIFIC LOWER EXTREMITY MUSCLE GROUPS IN HUMANS

A Thesis
Presented to
The Academic Faculty

by

Gregory Clark Henderson

In Partial Fulfillment
of the Requirements for the Degree
Master of Science in the
School of Mechanical Engineering

Georgia Institute of Technology
May 2012

PNEUMATICALLY-POWERED ROBOTIC EXOSKELETON TO EXERCISE SPECIFIC LOWER EXTREMITY MUSCLE GROUPS IN HUMANS

Approved by:

Dr. Jun Ueda, Advisor
School of Mechanical Engineering
Georgia Institute of Technology

Dr. Wayne Book
School of Mechanical Engineering
Georgia Institute of Technology

Dr. Minoru Shinohara
School of Applied Physiology
Georgia Institute of Technology

Date Approved: March 20th, 2012

ACKNOWLEDGEMENTS

I graciously thank my advisor, Dr. Jun Ueda, whose guidance and wisdom have helped me through my entire graduate school experience. I thank my committee members, Dr. Wayne Book and Dr. Minoru Shinohara, for their time and efforts. I am thankful for my colleagues here at Georgia Tech, particularly in the Bio-Robotics and Human Modeling Laboratory and the Machine Shop of the MRDC, for helping me on a range of topics I had not been familiar with prior. Finally, I would like to express gratitude to my family for believing in me and supporting me.

This project was made possible through generous funding and support from the United State's Science, Mathematics, and Research for Transformation (SMART) Scholarship.

.

TABLE OF CONTENTS

LIST OF TABLES

LIST OF FIGURES

LIST OF SYMBOLS AND ABBREVIATIONS

Symbol	*Meaning*
c	Weighting Factors for Minimization Function
g	Gravity Vector
f	Muscle Force Vector
f_{MAX}	Maximum Contracting Force of Muscle
i	*i*-th muscle
j	Number of Physical Joints
k_1	Static flow gain at zero load pressure drop
l_1	Length of Portion of Thigh
l_2	Length of Portion of Shank
l_3	Length of Cylinder at Fully Retracted Length
m_a, $\dot{m}_a$	Mass / Change in Mass of Air in Chamber side "a" of actuator
m_b, $\dot{m}_b$	Mass / Change in Mass of Air in Chamber side "b" of actuator
n	Number of Muscles Defined
r	Integer Number
u(*f*)	Cost (Minimization) Function
$\ddot{x}$	Horizontal Acceleration of Pelvis relative to Ground Fixed Frame
$\ddot{y}$	Vertical Acceleration of Pelvis relative to Ground Fixed Frame
A	Muscle Moment Arm Matrix
A_a	Cross-Sectional Area of Chamber Side "a" of Pneumatic Actuator
A_b	Cross-Sectional Area of Chamber Side "b" of Pneumatic Actuator
A_{rod}	Cross-Sectional Area of Piston Rod of Pneumatic Actuator
B	Pneumatic Actuator to Knee Moment Arm Matrix

$\mathbf{C}$	Centrifugal Effect Matrix
C_f	Discharge Coefficient of the Valve
C_r	Pressure Ratio
C_v	Coefficient of Viscous Friction
$\mathbf{F}$	Pneumatic Actuator Force Vector
$\mathbf{F}_{\boldsymbol{Actual}}$	Actual Force generated by Actuator
$F_{friction}$	Force from Friction
$F_{stiction}$	Force from Static Friction
F_A	Pneumatic Actuator Force Vector at Ankle Joint
F_H	Pneumatic Actuator Force Vector at Hip Joint
F_K	Pneumatic Actuator Force Vector at Knee Joint
I	Area of Spool Valve in Frequency Domain
K_I	Integral Gain
K_P	Proportional Gain
L	Length of Actuator
$\mathbf{M}$	Inertial Mass Matrix
$\mathbf{P}$	Pelvis Translation Matrix
PCSA	Physiological Cross Sectional Area
P_a	Pressure within Chamber Side “a” of Pneumatic Actuator
$\dot{P}_a$	Change in Pressure within Chamber Side “a” of Actuator
P_{atm}	Atmospheric Pressure
P_b	Pressure within Chamber Side “b” of Pneumatic Actuator
$\dot{P}_b$	Change in Pressure within Chamber Side “b” of Actuator
P_d	Downstream Pressure
P_u	Upstream Pressure

$P_{Actuator}$	Pressure within the chamber side of Pneumatic Actuator
$P_{Chamber}$	Pressure in Chamber
P_{Supply}	Supply Pressure
Q	Change in Pressure in Frequency Domain
R	Universal Gas Constant
T	Temperature of the Gas
$\mathbf{V}$	Coriolis Effect Matrix
X	Absolute Displacement of Piston Rod within Pneumatic Actuator
$\dot{X}$	Velocity of Piston Rod within Pneumatic Actuator
θ_A	Angle of Ankle (radians)
θ_C	Angle as Expressed through Law of Cosines (radians)
θ_H	Angle of Knee (radians)
θ_K	Angle of Hip (radians)
$\dot{\theta}_A$	Velocity of Ankle (radians/second)
$\dot{\theta}_H$	Velocity of Hip (radians/second)
$\dot{\theta}_K$	Velocity of Ankle (radians/second)
$\ddot{\theta}_A$	Acceleration of Ankle (radians/second^2)
$\ddot{\theta}_H$	Acceleration of Hip (radians/second^2)
$\ddot{\theta}_K$	Acceleration of Knee (radians/second^2)
σ_{muscle}	Specific Muscle Strength
τ	Time Constant of Pneumatic Cylinder
$\boldsymbol{\tau}_{ACTUATOR}$	Pneumatic Actuator Torque
$\boldsymbol{\tau}_{\text{MUSCLE}}$	Torque Applied by Musculotendon Actuators

SUMMARY

A control method is proposed for exercising specific muscles of a human's lower body. This is accomplished using an exoskeleton that imposes active force feedback control. The proposed method involves a combined dynamic model of the musculoskeletal system of the lower-body with the dynamics of pneumatic actuators. The exoskeleton is designed to allow for individual control of mono-articular or bi-articular muscles to be exercised while not inhibiting the subject's range of motion.

The control method has been implemented in a 1-Degree of Freedom (DOF) exoskeleton that is designed to resist the motion of the human knee by applying actuator forces in opposition to a specified muscle force profile. In this research, there is a discussion on the model of the human's lower body and how muscles are affected as a function of joint positions. Then it is discussed how to calculate for the forces needed by a pneumatic actuator to oppose the muscles to create the desired muscle force profile at a given joint angles. The proposed exoskeleton could be utilized either for rehabilitation purposes, to prevent muscle atrophy and bone loss of astronauts, or for muscle training in general.

CHAPTER 1

INTRODUCTION

As humans, we constantly use our bones and muscles to accomplish everyday tasks. To some, using their muscles is strictly for accomplishing necessary tasks; to others, they could just enjoy the feeling of building up a good sweat from exercise. Regardless of the reasoning, it is vital to utilize your muscles and exercise them for a long and healthy life.

Certain situations in life however bring a need to exercise for a specific purpose. This could mean just a general exercising of a certain limb for a particular task or even further controlling specific muscles to train for specific tasks. Examples of specific tasks could be training your legs for maximum endurance for a marathon run or even just a sense of basic mobility when coming back from space.

Regarding applications such as space, as humans inevitably extend their domains to the reaches of space; either traveling to Mars, a space station, etc., they must account for the effects of micro-gravity on their bones and muscles. A human's physiology adapts to the physical environment they are currently in. As this environment changes from an Earth to a microgravity environment such as space, this leads to muscle atrophy and bone loss due to the loss of the constant force of gravity [6].

In humans, there is a system of cells that work in unison to break down old bone and create new bone in its place. The cells that reabsorb and break down old bone are osteoclasts and the cells that build new bone are osteoblasts. The cells for a normal, healthy adult on Earth work to create an equilibrium where the rate of bone loss is equal to the rate of bone creation. New bone is normally deposited in proportion to the compressional loads directed on a bone. In space however, with little to no applied loads

due to micro-gravity, bone formation decreases and net bone loss occurs. Some causes of bone loss on Earth (osteoporosis) occur due to age, lack of physical activity, malnutrition, and lack of estrogen secretion in women after menopause. For either a space or earth-based bone loss case, it is useful to understand why bone loss occurs to find a solution for this problem. Research on the topic of skeletal unloading and its effects on bones have been investigated by Holton et al. [16], [17] and research on muscle atrophy due to micro-gravity has been investigated by Caiozzo et al. [5].

1.1 Motivation

The primary motivation for this research is to determine how to create an actively-controlled exercise machine for muscle-isolation exercise. The motivations and potential applications for this research depends on being on earth or up in space. On earth, a muscle-isolation exercise machine could bring an extra degree of freedom to a physical therapist to have more control over what types of muscle forces they desire for their patients. It could also be used in a gravity environment for sports training purposes, or for the fitness enthusiast, a new way of exercising.

In space, the motivation behind this research involves helping astronauts to more effectively exercise to mitigate the effects of microgravity on bones and muscles. This would help to shorten rehabilitation time when returning to a higher gravity environment, minimize bone loss, and preventing injuries such as bone fractures. Bone fractures could jeopardize missions such as to Mars where medical help is limited and are especially dangerous.

1.2 Research Objectives

The proposed exoskeleton uses a dynamic model of the musculoskeletal system of the lower leg combined with the dynamics from a pneumatic actuator to provide resistive forces to the muscle forces. The exoskeleton will use a quasi-dynamic (useful for slow to moderate human movement speed) force-feedback control method to determine how the pneumatic actuators should apply forces at desired positions and times.

CHAPTER 2

BACKGROUND AND LITERATURE REVIEW

2.1 Muscle Atrophy and Bone Loss

There are many different machines that are utilized today by the National Aeronautics and Space Administration (NASA) to counteract the effects of micro-gravity such as a treadmill, a bicycle ergometer, iRED (interim resistive exercise device) [22], etc. These machines have limitations, however, such as being geometrically large, heavy (leading to higher launching costs), and are series exercise machines. A series exercise machine is a device in which the user cannot actively carry out mission-related tasks and exercise at the same time. The efficacy of using methods such as these were investigated by Trappe et al. [27] where astronaut subjects exercised as much as 2.5 hours a day for 6-7 days a week (approximately 7-10% of available time spent awake for crewmembers) while aboard the International Space Station for six months. The results after their return to Earth were muscle performance losses of ~20-29% while a control group of bed-rest subjects (without countermeasures) had muscle performance losses of ~40% during the same time frame. This illustrates a need for methods of exercise that are more effective and time-efficient in lessening the adverse effects of micro-gravity.

The proposed method of overcoming some of the limitations of current exercise equipment would be a pneumatically-powered robotic exoskeleton. The design would be low in size and weight, modular for differently sized people, allow adjustable physical parameters (such as forces exerted), and act as a parallel exercise device (exercising while able to accomplish other activities).

2.2 Assistive/Resistive Exoskeletons

Extensive research has been created over the years in regards to assistive robotic exoskeletons such as the BLEEX exoskeleton [13], HAL-5 exoskeleton [12], etc. Contributions towards assistive exoskeletons have included modeling of human anatomy [19], [21], modeling of various actuation technologies [15], and control of these systems [15], as well as many others.

There have been investigations into *resistive robotic exoskeletons and resistive exercise machines* as well such as Furusho et al. [10] and Book et al. [4] but fewer research investigations into selectively controlling the individual muscle forces. The idea of a *resistive robotic exoskeleton* comprises the understanding of the biomechanical structures in question; in this case, the lower extremities of a human. Research into a *resistive robotic exoskeleton* for the upper body was investigated by Ueda et al. [28].

CHAPTER 3

DYNAMIC MODEL OF HUMAN LEG AND ROBOTIC EXOSKELETON

To accurately describe the forces/torques generated by the robotic exoskeleton onto the lower extremity, a dynamic equation is necessary to model the relationship between the two parts. Fig.1 shows a model of the 3-DOF musculoskeletal system of a human's lower limb.

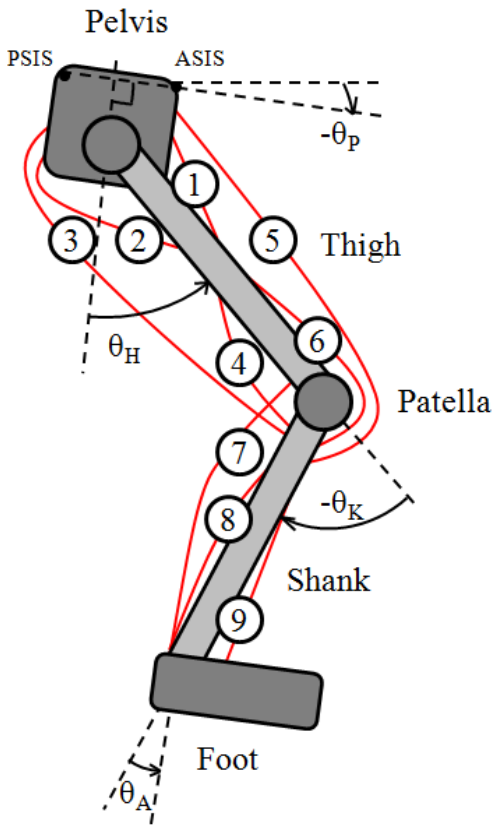

Figure 1. Musculoskeletal Model of Human Lower Extremity, Hip angle defined as angle between long axis of thigh and perpendicular line connecting the ASIS and PSIS

3.1 Musculoskeletal Model of Human Lower Extremity

This musculoskeletal model was derived from [18] and breaks the muscles in the leg down into nine distinct muscle groups. These groups are defined in Table 1.

Table 1

SPECIFIC MUSCLES AND MAXIMUM ISOMETRIC MUSCLE FORCE

Muscle "i"	MUSCLE NAME	f_{MAX_i} (N)
1	Illiopsoas	1850
2	Gluteus Maximus/Medius	2370
3	Hamstrings	2190
4	Bicep Femoris (Short Head)	400
5	Rectus Femoris	1000
6	Vasti	5200
7	Gastocnemius (Lat and Med. Head)	1600
8	Soleus (Plantarflexion)	3600
9	Tibialis Anterior (Dorsaflexion)	1100

From [15], a modified equation of motion was created to dynamically model the swinging motion of the leg and is given by

$$\mathbf{M}\begin{bmatrix}\ddot{\theta}_H\\ \ddot{\theta}_K\\ \ddot{\theta}_A\end{bmatrix} = \mathbf{C}\begin{bmatrix}\dot{\theta}_H^2\\ \dot{\theta}_K^2\\ \dot{\theta}_A^2\end{bmatrix} + \mathbf{V}\begin{bmatrix}\dot{\theta}_H\dot{\theta}_K\\ \dot{\theta}_H\dot{\theta}_A\\ \dot{\theta}_K\dot{\theta}_A\end{bmatrix} + \mathbf{P}\begin{bmatrix}\ddot{x}\\ \ddot{y}\end{bmatrix} + \mathbf{g} + \boldsymbol{\tau}_{\text{MUSCLE}} - \boldsymbol{\tau}_{\text{ACTUATOR}} \qquad (1)$$

where θ_H, θ_K, and θ_A are the hip, knee, and ankle joint angles respectively; $\tau_{\text{MUSCLE}} = [\text{M}_\text{H} \quad \text{M}_\text{K} \quad \text{M}_\text{A}]^\text{T}$ are the torques applied by the musculotendon actuators, $\tau_{\text{ACTUATOR}} = [\tau_\text{H} \quad \tau_\text{K} \quad \tau_\text{A}]^\text{T}$ are the torques supplied by the exoskeleton's actuators, x and y are the horizontal and vertical displacements of the pelvis relative to a ground-fixed reference

frame; **M** is the inertial mass matrix; **C** is the Centrifugal effect matrix; **V** is the Coriolis effect matrix; **P** is the Pelvis translation matrix; and **g** is the Gravity vector. The constants and coefficients used within the equations of motion shown above are found in [18]. The physical parameters of the human (such as leg length, mass, moment of inertia, etc.) were taken from [19] and [21] and are found in Table 2.

Table 2

ANTHROPOMETRIC DATA OF SHANK, THIGH, AND ANKLE

	Length (m)	Distance from proximal end to Center of Mass (m)	Mass (kg)	Moment of Inertia (kg-m^2)
Thigh	0.5	0.244	10	0.2431
Shank	0.45	0.279	3.5	0.0476
Ankle	N/A	*0.08	0.99	0.005

* Indicates hypotenuse length due to Center of Mass being off-center of Shank axis

When each of these muscles defined in the musculoskeletal model in Fig. 1 are multiplied by their respective moment arms, the output will be the total muscle torques created at each joint and is given by

$$\boldsymbol{\tau}_{\text{MUSCLE}} = \mathbf{A}(\theta)^{j\times n}\mathbf{f}^{n\times 1} \tag{2}$$

where $\mathbf{A}(\theta)^{j\times n}$ is the moment arm matrix for "*j*" number of physical joints where in this case *j* = {Hip "H", Knee "K", Ankle "A"}, and "*n*" number of muscles; and $\mathbf{f}^{n\times 1}$ is the force vector for "*n*" number of muscles. The $\mathbf{A}(\theta)^{j\times n}$ matrix was created by a combination of various different studies on the hip, knee, and ankle joints, and the muscles and moment arms involved with each of these joints. The moment arm matrix is

found in Table 3 and is a modified version of the matrix used in [18] using the above-mentioned studies.

Table 3

MOMENT ARMS $A_{j\times n}$ OF MUSCLE GROUPS $n = 1\ldots 9$ (IN METERS, θ IN RADIANS; VALUES NOT SPECIFIED ARE EQUAL TO ZERO)

JOINT:	EQUATION:
Hip Joint:	$A_{H1} = 0.00233\theta_H^2 - 0.00223\theta_H - 0.0275$
	$A_{H2} = -0.0098\theta_H^2 - 0.0054\theta_H + 0.0413$
	$A_{H3} = -0.020\theta_H^2 - 0.024\theta_H + 0.055$
	$A_{H5} = 0.025\theta_H^2 + 0.041\theta_H + 0.040$
Knee Joint:	$A_{K3} = -0.0098\theta_K^2 - 0.021\theta_K + 0.028$
	$A_{K4} = -0.008\theta_K^2 - 0.027\theta_K + 0.014$
	$A_{K5} = -0.058\exp(-2.0\theta_K^2)\sin(-\theta_K) - 0.0284$
	$A_{K6} = -0.070\exp(-2.0\theta_K^2)\sin(-\theta_K) - 0.0250$
	$A_{K7} = 0.018$
Ankle Joint:	$A_{A7} = 0.053$
	$A_{A8} = 0.035$
	$A_{A9} = 0.013(\theta_A + .637_{\dagger}) - 0.035$
	† : Ankle Position offset defined in [19]

3.2 Wearable Robotic Exoskeleton

The equation for the torque that the actuator produces is similar to the equation for the muscle torques and is defined as

$$\boldsymbol{\tau}_{ACTUATOR} = \mathbf{B}(\theta)^{3\times3}\mathbf{F}^{3\times1} \tag{3}$$

where $\mathbf{B}(\theta)^{3\times3}$ is an invertible moment arm matrix due to not having redundant muscles components as $\mathbf{A}(\theta)^{j\times n}$ does. The components of $\mathbf{B}(\theta)^{3\times3}$ are defined by the actuator's attachment points onto the body; $\mathbf{F}^{3\times1} = [\mathrm{F_H} \quad \mathrm{F_K} \quad \mathrm{F_A}]^{\mathrm{T}}$ is the general case force vector for the forces produced by the pneumatic actuators to counteract the muscle forces produced at the hip, knee, and ankle joints. For this specific case, the force vector is

defined as $\mathbf{F}^{3\times1} = [\, f(\mathrm{F_K}) \quad \mathrm{F_K} \quad 0]^{\mathrm{T}}$ where the actuator at the knee joint produces force and the hip actuator produces a force as a function of this knee force. The force from the hip actuator is used to counteract the moment created by just the actuator knee force on the body to keep the hip at a constant position. This removes the need to account for the target muscle in contributing to both the force created to oppose the knee actuator as well as keeping the hip in a fixed position. For this specific case, the relationship between moving the knee with an actuator attached to it and worrying about torque about the hip to keep the hip angle constant is decoupled. This then focuses only on the muscles to act against the one actuator acting on the joint. An experiment specific figure is shown below in Fig. 2 to illustrate this with the various actuators at different joints.

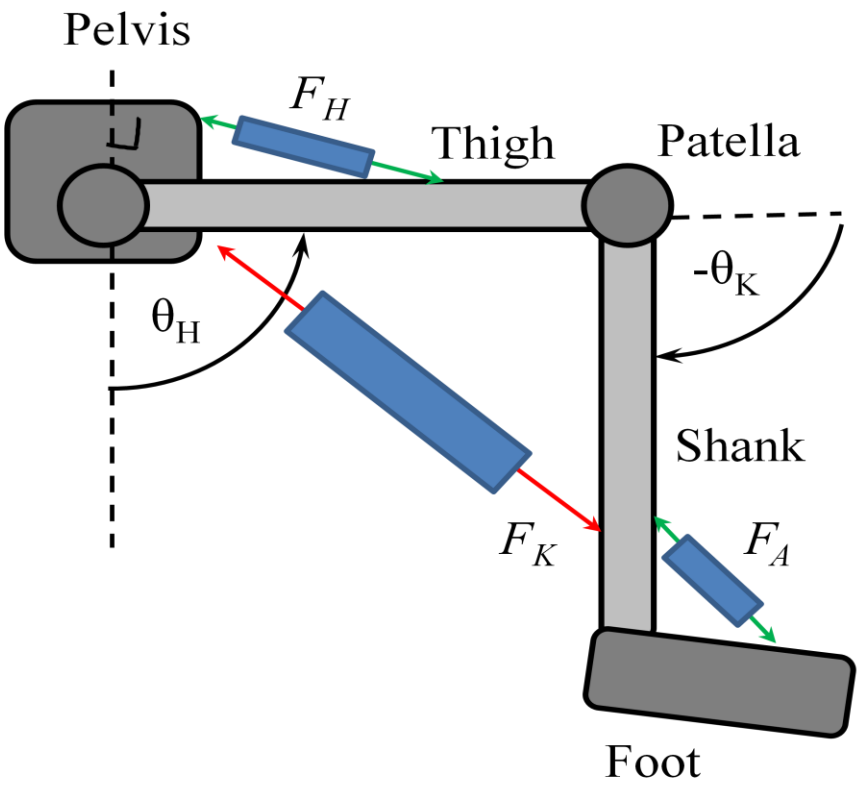

Figure 2. Skeletal Model with Pneumatic Actuators attached

CHAPTER 4

DYNAMIC MODEL OF PNEUMATIC ACTUATOR

For the purposes of this study, pneumatic actuators were chosen to create the resistive forces against the muscle forces due to their active stiffness characteristics that allow the forces they produce to be altered whenever desired. A wealth of research has been produced to dynamically model the pneumatic actuators as well as to control the dynamic characteristics of the actuator such as force and stiffness. The work of Shen et al. shows how using two 3-way proportional valves rather than one 4-way valve can be used to independently control the force and stiffness characteristics of a pneumatic actuator. It accomplishes this by changing the equilibrium point of the actuator (point of zero force) or pressurizing both chamber sides of the actuator to modify the "spring" stiffness [15]. A pneumatic actuator is modeled in Fig. 3.

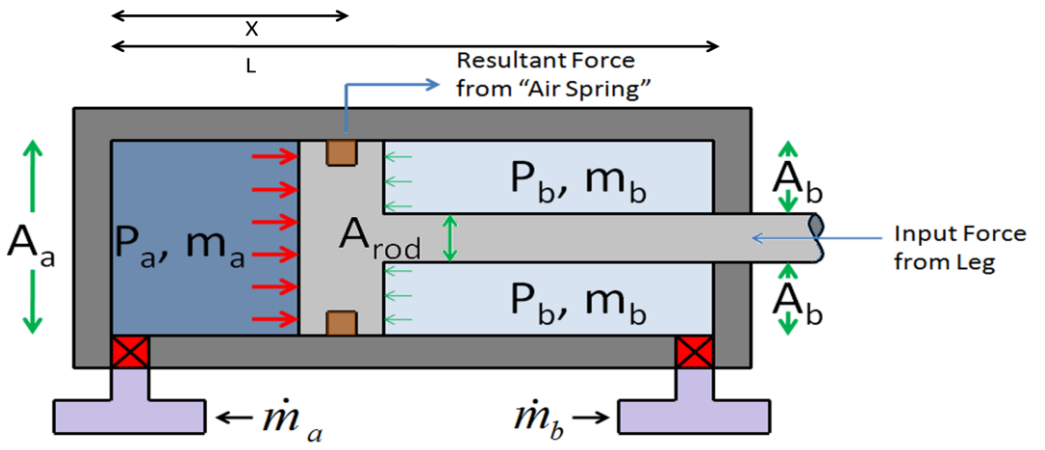

Figure 3. Schematic of Pneumatic Actuator

4.1 Pneumatic Actuator

Here, P_a and P_b are the absolute pressures inside each chamber of the actuator; m_a, m_b, and $\dot{m}_a$, $\dot{m}_b$ are the masses of air and change of masses on each side of the

piston respectively, A_a and A_b are the effective areas of each side of the piston; and A_{rod} is the cross-sectional area of the piston rod. Based on the schematic shown in Fig. 3, the force generated by the actuator is given by

$$F_e = P_a A_a - P_b A_b - P_{atm} A_{rod}, \; e = \{H, K, A\} \tag{4}$$

$$F_{Actual} = F_e + F_{friction} \tag{5}$$

where P_{atm} is atmospheric pressure and $F_{friction}$ is the resistive force of friction against movement. To understand how quickly the pneumatic actuator would be able to respond to the torques created by the muscles, the Force equation is differentiated with respect to time. This change in force is utilized in the closed-loop control law discussed in the next chapter and does not account for frictional forces at this point.

$$\dot{F}_e = \dot{P}_a A_a + \dot{P}_b A_b, \; e = \{H, K, A\} \tag{6}$$

This equation allows us to determine the hardware's limit of how quickly it can change the output force. The change in output force is a function of the summation of the two proportional valves and the changes in pressure they can create. The pressure they can create is a function of the cross-sectional area open of the proportional spool valve used in the experimental setup and is discussed in the next section.

4.2 Mass Air Flow

To model the change in pressures formed by the valves, it is necessary to account for the dynamics of mass being let into or out of the cylinder and how this will affect the resulting force of the cylinder. This mass flow, or the rate flowing in and out of the

cylinder, is a function of the orifice area exposed open of the spool valve and the upstream and downstream pressures and is defined in the form

$$\dot{m} = A_{spool}\Psi(P_d, P_u) \tag{7}$$

where A_{Spool} is the cross sectional area of the spool open due to a voltage applied to the proportional valve. The spool valve's position will dictate whether the system will be charging (air flowing into the side of the chamber), or discharging (air flowing out of the chamber). From here, the upstream and downstream pressures are dependent on whether it is a charging or discharging case. The two cases are defined as follows:

Charging (air flowing in to cylinder): $P_d = \mathrm{P_{Supply}}$, $P_u = \mathrm{P_{Chamber}}$

Discharging (air flowing out to atmosphere): $P_d = \mathrm{P_{Chamber}}$, $P_u = \mathrm{P_{atm}}$

For the function shown above as $\Psi(P_d,P_u)$, it is defined as a nonlinear piecewise function that varies based on a pressure ratio which will indicate whether the pneumatic valve is operating in a choked (sonic) or unchoked (subsonic) flow state. This pressure ratio that divides between choked and unchoked airflow is defined as:

Transitional Pressure Ratio of Air → $C_r = P_d/P_u = 0.528$

Where the following equation is expressed in [22]

$$\Psi(P_u, P_d) = \begin{cases} \text{if} \quad \dfrac{P_d}{P_u} \le C_r \ (\textit{choked}) & \sqrt{\dfrac{\gamma}{RT}\left(\dfrac{2}{\gamma+1}\right)^{(\gamma+1)/(\gamma-1)}}\, C_f P_u \\ \text{if} \quad \dfrac{P_d}{P_u} > C_r \ (\textit{unchoked}) & \sqrt{\dfrac{2\gamma}{RT(\gamma-1)}}\sqrt{1-\left(\dfrac{P_d}{P_u}\right)^{(\gamma-1)/\gamma}\left(\dfrac{P_d}{P_u}\right)^{(1/\gamma)}}\, C_f P_u \end{cases} \tag{8}$$

and C_f is the discharge coefficient of the valve that accounts for irreversible flow conditions, γ is the ratio of specific heats, R is the universal gas constant, and T is the temperature of the gas at the orifice. For air, γ = 1.4 and R = 287 J/Kg-K.

Once mass air flows are known, from [22], (6) can be expressed as a function of mass flows and the cylinder position for better control of the change in force of the actuator and tracking control.

$$\dot{\mathrm{F}}_e = \frac{RT}{\frac{L}{2}+X}\dot{m}_a - \frac{RT}{\frac{L}{2}-X}\dot{m}_b - \frac{P_a A_a \dot{X}}{\frac{L}{2}+X} - \frac{P_b A_b \dot{X}}{\frac{L}{2}-X} \qquad e = \{\mathrm{H},\mathrm{K},\mathrm{A}\} \tag{9}$$

where L is the length of the actuator, X is the cylinder position, and $\dot{X}$ is the velocity.

However, under the current assumption from empirical testing the pneumatic actuator responds faster in the change of force than what is desired by the change of actuator force for the desired force profile. Because of this, $\dot{F}_l$ from the pneumatic cylinder will not be the hindrance towards tracking speed at current velocity levels experimented with.

4.3 Valve Modeling

There are various methods to model the valve but since this experiment will be run at low frequencies, a first-order model should suffice [26].

A first-order transfer function is used to describe the proportional spool valve and is described as:

$$\frac{Q}{I}(s) = \frac{k_1}{\tau s + 1} \tag{10}$$

Where Q(s) = $\mathcal{L}\left(\dot{P}_{Actuator}(t)\right)$, I(s) = $\mathcal{L}\left(A_{Spool}(t)\right)$, $\mathcal{L}$ denotes a Laplace Transform, $\dot{P}_{Actuator}$, is the change in the pressure within the one chamber side of the pneumatic actuator, k_1 is the valve's static flow gain at zero load pressure drop / the gain to get the units in the correct format, and τ is the apparent time constant.

This transfer function was then used for an experimental test that was run involving a step function to see how quickly the valve responds to change from ambient pressure within the valve to the supply pressure. After running this experiment, the following first-order equation is used to fit to the data collected:

$$P_{Actuator}(t) = P_{Supply}\left(1 - e^{-t/\tau}\right) \tag{11}$$

where $P_{Actuator}$ is the Pressure within the chamber side of the Pneumatic Actuator, t is the time after the unit step is triggered, and P_{Supply} is the supply pressure given to the system. To obtain the time constant for the system, the experiment tested for the fastest pressure change that the valve could create within a fixed amount of volume of the pneumatic cylinder. Utilizing the ideal gas law with temperature and volume constant, the pressure change is a function of the change in mass flow into the cylinder. Fig. 4 below shows how the change in pressure increases as you open the proportional spool valve more. The maximum pressure change for one valve is shown in the curve that has the input voltage signal of 10 volts. Here the time constant "τ" was experimentally found to be around 0.1 seconds.

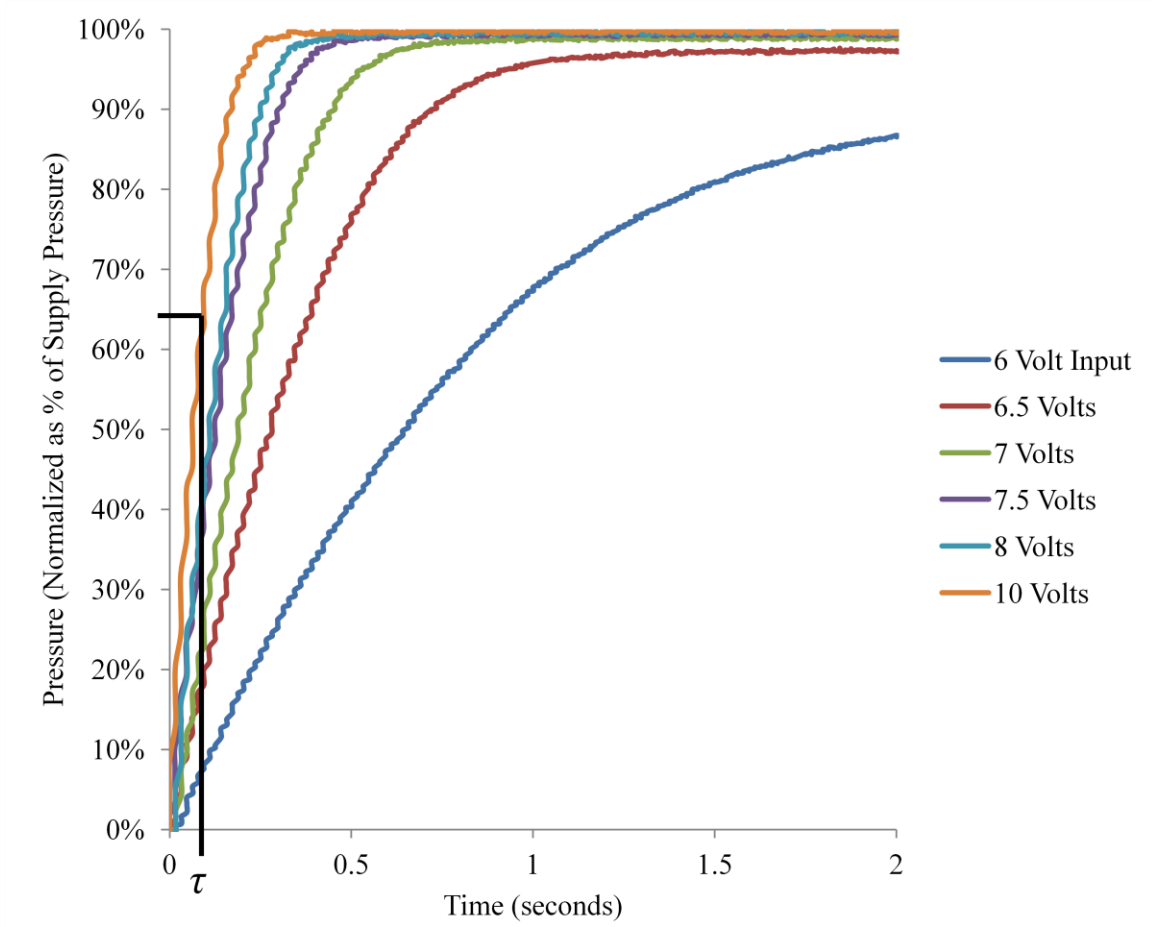

Figure 4. Determining experimental time constant of valve as the voltage is increased, the valve is opened more and the pressure increases into the pneumatic cylinder quicker. A time constant was found experimentally around 100 msec

4.4 Friction (Stiction/Viscous) Compensation

Friction is a common topic of interest regarding modeling and controlling pneumatic actuators. For the purposes of this experimental system, both static friction (stiction) and dynamic (viscous) friction are addressed. Static friction represents the amount of force needed to have the actuator begin to move. The static friction is a function of the seals and lubrication used within the pneumatic cylinder assembly and is normally considered as a fixed value. As a side note, there seems to be more stiction at

the end stops of the actuator's stroke, but this will not be addressed in this research. Once the rod pushes past the stiction force and begins to move, the forces imposed against the rod then transition to viscous force. Viscous force is a function of the speed at which the system moves and is normally based upon interactions of cylinder components as well as the potential of compressibility of the air within the cylinder itself.

There have been various different methods of modeling the effects of friction [1], [24], [32] that vary in regards to complexity. Since this research involves a control system running on-line, it is desired to have a simplified friction model to account for friction but not being exceedingly computational expensive. The model used in this experiment is made of two parts that address both the stiction and viscous components of the friction and is addressed in the next Chapter. For the actuator used in this experiment, (Bimba 097-DP), it has Nitrile Rubber seals which will be a factor in the frictional force. Frictional forces will be discussed in the next chapter.

CHAPTER 5

FORCE CONTROL OF PNEUMATIC ACTUATOR

5.1 Open Loop Force Control

Once a combined model of the pneumatic actuator and the human musculoskeletal system is created, a control method is necessary to accurately track a reference force. During the initial setup phase, it was discovered that the system was able to respond to a step-command within milliseconds. This prompted the assumption to ignore the effects of the upper bound of how quickly air can flow into the cylinder ($\dot{m}$ equations from previous section) and assume that any force desired can be realized within small fractions of a second and ignore the negligible effects of the $\dot{m}$ dynamics.

In the experimental setup, it was necessary to determine hardware limitations for the system. An open loop experiment was run sending sinusoidal frequencies to the proportional valves and measuring the output force from the force sensor. It is of interest to determine what ranges of forces are realizable through a frequency sweep of 1 to 5 Hz. This is shown in Fig. 5.

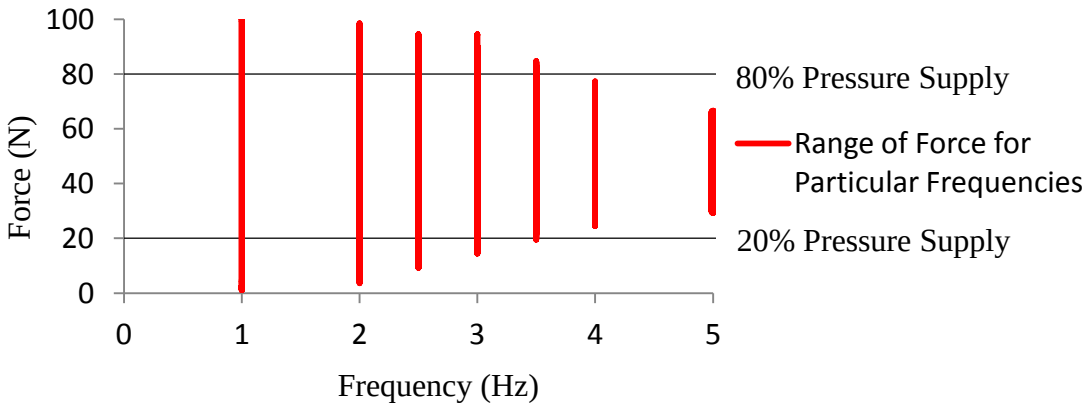

Figure 5. Range of forces from 1 to 5 Hz. Open loop force control to determine maximum force ranges

5.2 Closed Loop Force Control

Using this knowledge, the next step was to create a closed-loop force feedback controller using a Proportional-Integral controller (discussed later in the chapter). A block diagram of the closed-loop controller is shown in Fig. 6.

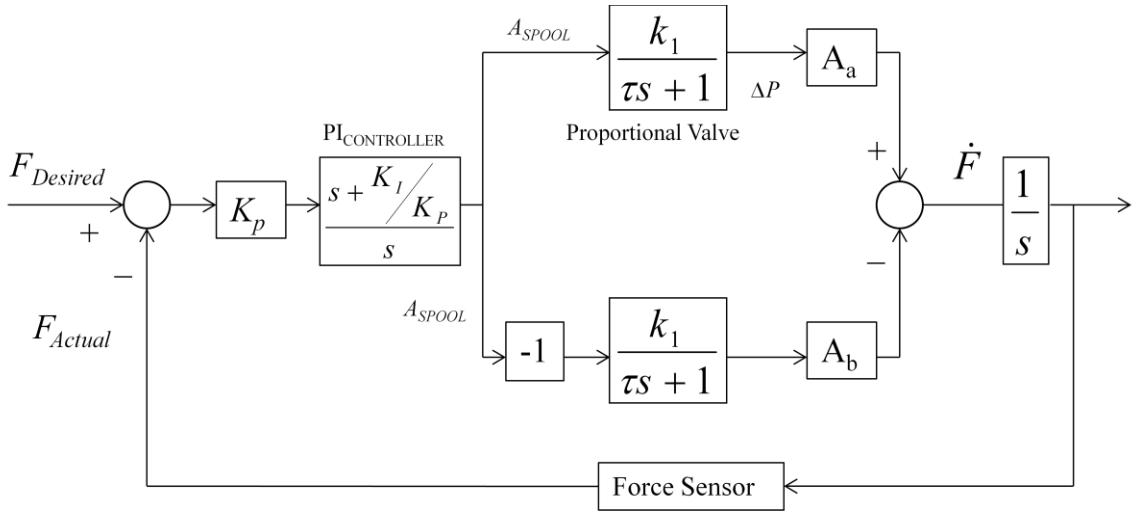

Figure 6. The Closed-Loop Force Feedback with PI Control

The model determines the change in pressures created from the valves based upon how much their spool valves are opened. These are then multiplied by their respective effective cross-sectional areas of each side of the piston to determine the change in force of the actuator. K_I and K_P are the Integral and Proportional Gains for the PI Controller discussed in the next section

5.2.1 Stability Check of System using Root Locus Method

To confirm stability for a closed loop system, we use the root locus method using the dynamics of the proportional valves used for a fixed pneumatic cylinder position.

From here, a root locus plot using the valves can be created from the pole created by the proportional valve "plant", the pole created from integrating the change in Force, and a Proportional-Integral (PI) Controller. A PI Controller is desired to decrease the rise time of the system to have it respond quicker for tracking a desired force and to decrease the steady-state error of the system. The model that is then used for the root locus plot is a simplified model of Fig. 6 and is shown below in Fig. 8. The Root Locus plot is shown in Fig. 9 below:

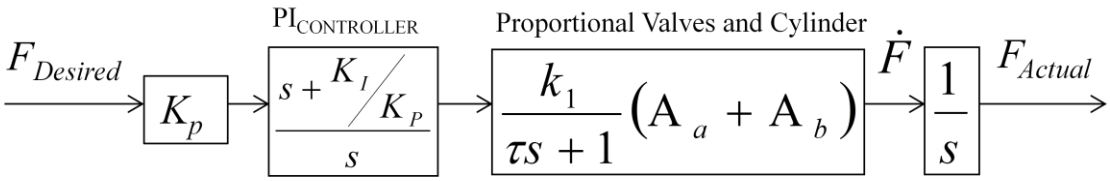

Figure 7: Simplified system model for Root Locus

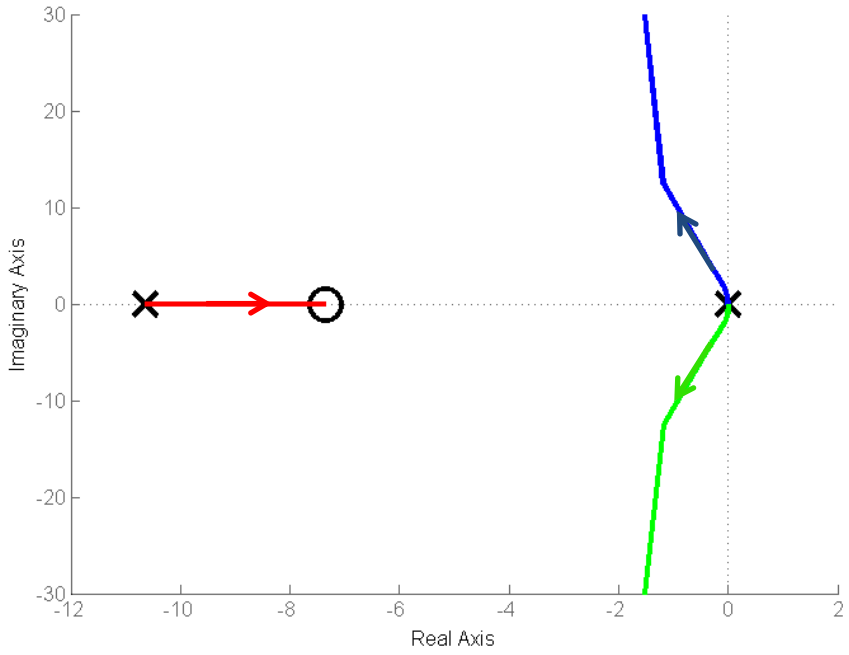

Figure 8. Root Locus of the Two Valves and a PI controller. There are two poles at the origin, one pole at $-1/\tau$ and one zero at $K_I/K_P = -7.5$

From this Root Locus Plot, it is shown that using a PI controller that the system is stable due to the poles and zeros being all on the negative real axis. The pole for the proportional valve is a function of the time constant and is determined experimentally. It was found that as long as the zero created by K_I/K_P (gain values of proportional and integral terms) is bounded between 0 and $-1/\tau$ that the system should be stable under current modeling assumptions so many different values of K_I/K_P could be used. Outside of the region (i.e. $K_I/K_P < -1/\tau$) that the two asymptotic curves coming from the two poles at the origin cross into the positive real plane and would cause instability.

5.3 Performance Analysis

To show that this method of force control for the system would be a viable option, various experiments were conducted at tracking a sinusoidal force at varying frequencies for performance analysis. For the purposes of this research, we wanted the system to be able to respond faster than a normal human's exercise frequency under load. This movement was found to be < 0.5 Hz for the range of motion of the knee. This was a benchmark created to show that if the system could respond at this frequency, the method would suffice. The system is meant to track a desired force that will be created from an iterative method shown in a Chapter 7. The values for K_I and K_P for the Controller were determined empirically using the root locus plot as a guide to yield a resultant force that matched as close as possible the reference force signal. These Proportional and Integral gains were then used for the set of all the Force Control Frequencies experimented with for the tracking force-control runs.

The closed-loop experiment was run to determine how well the force feedback control could track a sinusoidal force signal oscillating between 20% and 80% of the supply pressure at various frequencies. These plots are shown below in Fig. 7.

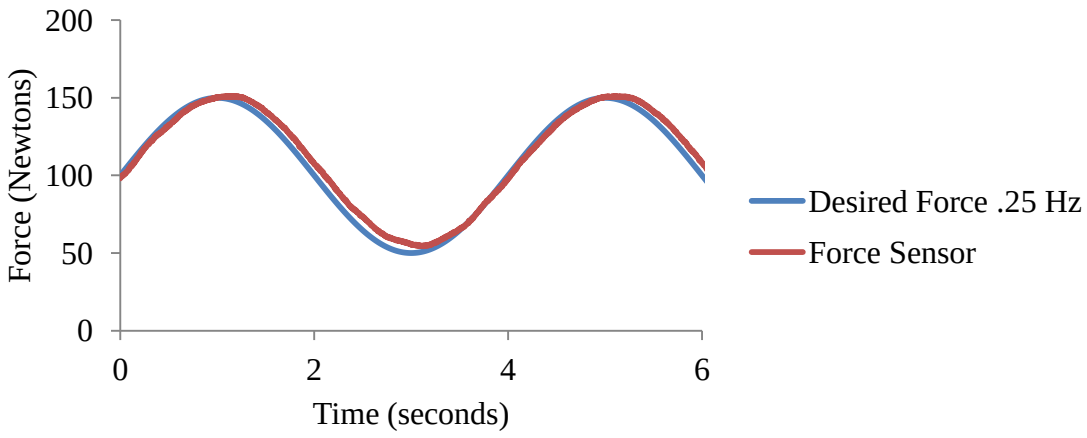

a.) 0.25 Hz Frequency

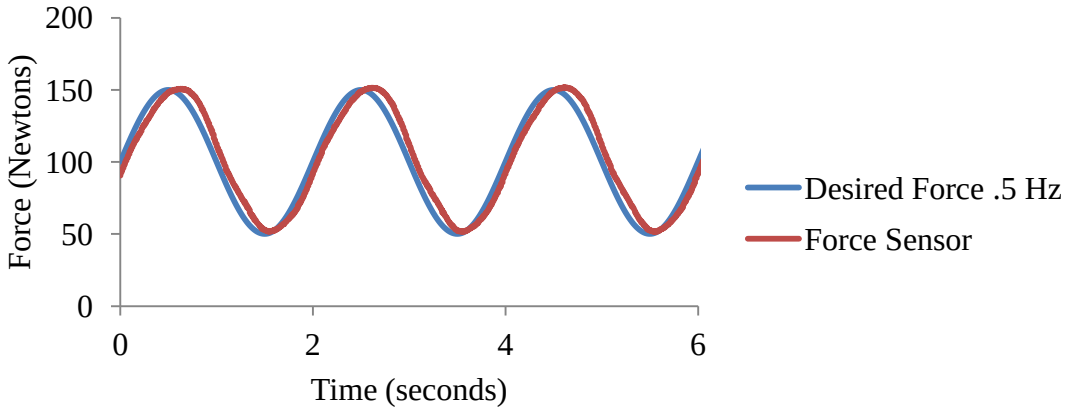

b.) 0.5 Hz Frequency

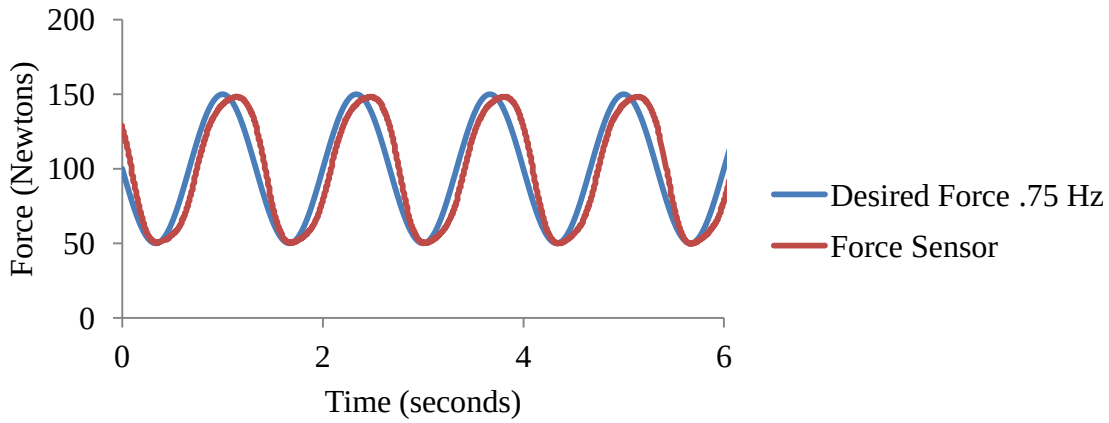

c.) 0.75 Hz Frequency

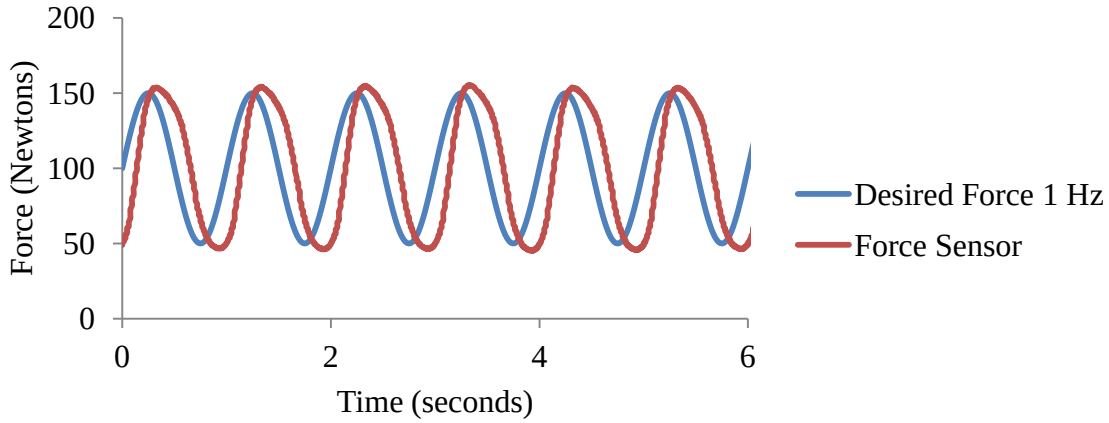

d.) 1 Hz Frequency

Figure 9. Closed-Loop Force Feedback Control following a sinusoidal reference force oscillating between 20% and 80% of supply pressure. The figures range in frequency of .25 Hz to 1 Hz. a.) .25 Hz, b.) .5 Hz, c.) .75 Hz, d.) 1 Hz

From these results, it is determined for a closed-loop response that the system can reasonably track a sinusoidal force at a fixed position of the pneumatic cylinder to at least a frequency of 1 Hz. For frequencies higher than 1 Hz, there seems to be more phase lag and less of an ability to track the force reference signal.

5.4 Friction Modeling

To create a more accurate model for tracking force control, it is necessary to account for the various types of friction throughout the movement of the pneumatic actuator. For this, we have two methods to account for both stiction and viscous friction. For the stiction component, originally a saw-tooth wave was used to slowly increase the force to see when the system would begin to move. Once the system began to move, the force it took to move the system was noted.

To account for this in the control loop, the reference force for the closed-loop system has an offset value of a dither command to produce a small amount of dither. This dither then will keep the system vibration minutely to help to break the static friction component so a user will be able to begin to move the pneumatic cylinder at a lowered static friction force.

When the user transitions from zero movement to small velocities, the system will now modify the given reference force as a function of the piston rod velocity. For this Force Control model, we use the following model for friction:

$$F_{friction} = \begin{cases} F_{stiction} & if\ \dot{X} = 0 \\ C_v\dot{X} & if\ |\dot{X}| > 0 \end{cases} \tag{12}$$

where C_v is the coefficient of viscous friction. C_v found empirically by using the experimental setup to run in position-control mode and using a triangular wave at various frequencies as the reference signal and measuring the force output. A triangular wave was chosen to create a constant velocity to either extend or retract the pneumatic rod. The plot of Pneumatic Cylinder velocity versus the Force needed to track the Position Signal is shown in Fig. 10.

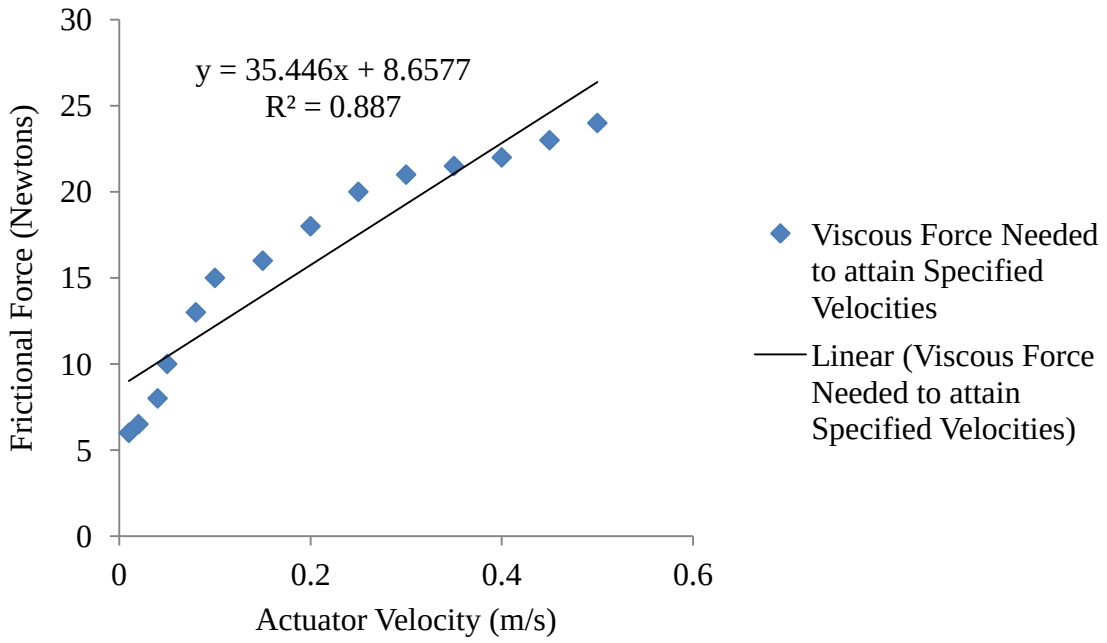

Figure 10. Sweeping of various velocities of the pneumatic cylinder and plotting the forces needed to track the position signal; Slope would be the empirical value of C_V

For this position control test, a small dither signal was added to the position reference signal to keep the system constantly vibrating minutely to focus only on the viscous friction component and not the stiction component. A linear trend line was then fitted to the data to then be used by the LabVIEW software later on for Viscous Friction Compensation. The trend line used for the Viscous Friction Compensation potentially could be fitted with a higher order polynomial instead. This would be to account for non-modeled or non-measurable parameters such as force created due to compression of the fluid, forces created by the specific manufacturing interface between the piston's seal to the sidewall of the internal chambers of the piston, etc that are shown in experimental data. This would require however a need for a non-linear friction model to justify fitting a non-linear curve to the experimental data.

CHAPTER 6

OPTIMIZATION METHODS TO DETERMINE MUSCLE FORCES

6.1 Simplified Model

With the parameters of the dynamics now fully defined, it is useful to rearrange (1) to solve for the Muscle Torques. In the general case, all terms from (1) would be used for the optimization and is given as:

$$\tau_{\text{MUSCLE}} = \mathbf{M}\begin{bmatrix}\ddot{\theta}_H \\ \ddot{\theta}_K \\ \ddot{\theta}_A\end{bmatrix} - \mathbf{C}\begin{bmatrix}\dot{\theta}_H^2 \\ \dot{\theta}_K^2 \\ \dot{\theta}_A^2\end{bmatrix} - \mathbf{V}\begin{bmatrix}\dot{\theta}_H\dot{\theta}_K \\ \dot{\theta}_H\dot{\theta}_A \\ \dot{\theta}_K\dot{\theta}_A\end{bmatrix} - \mathbf{P}\begin{bmatrix}\ddot{x} \\ \ddot{y}\end{bmatrix} - \mathbf{g} + \tau_{\text{ACTUATOR}} \qquad (13)$$

From experimental testing, it was found with one joint moving at a constant speed that the velocity terms are quite small and the accelerations correspondingly are quite small in relation to the torques generated by gravity about the knee joint. For this research where the case is that the velocities are small and acceleration negligible (< 3% of total desired muscle torque), the general case turns into a simplified, specific case for optimization.

$$\tau_{\text{MUSCLE}} = -\mathbf{C}\begin{bmatrix}\dot{\theta}_H^2 \\ \dot{\theta}_K^2 \\ \dot{\theta}_A^2\end{bmatrix} - \mathbf{g} + \tau_{\text{ACTUATOR}} \qquad (14)$$

Validation as to why acceleration may be neglected in the calculations is found in Fig. 11.

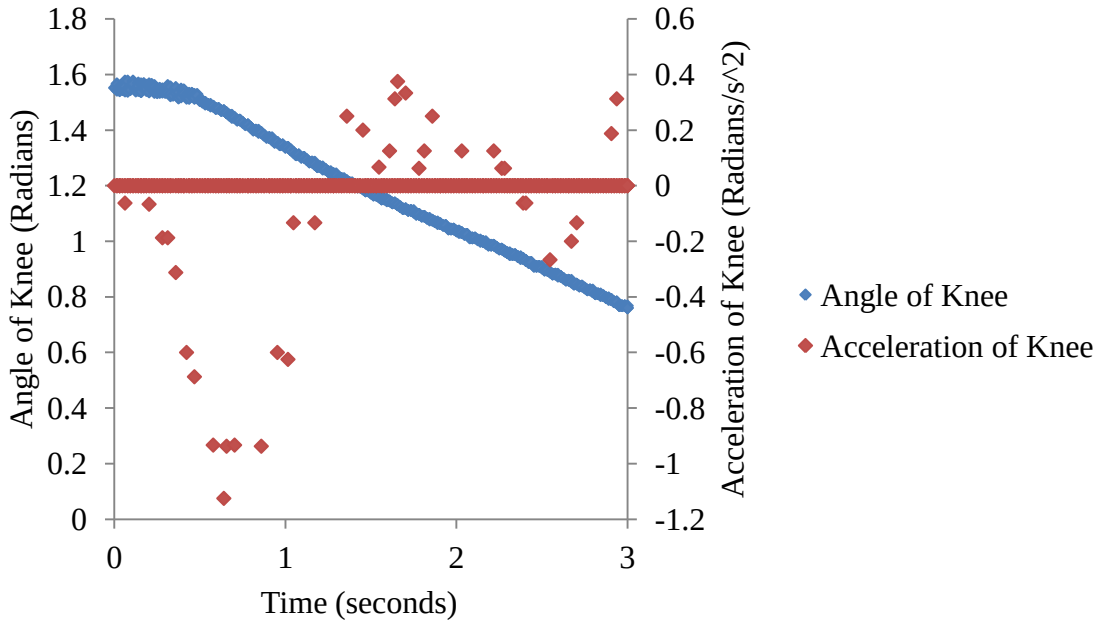

Figure 11. The acceleration values found in this experiment when multiplied by the inertia matrix were found to contribute less than 3% of the total desired muscle torque. If the acceleration becomes larger, the desired muscle torque will need to accommodate for it.

6.2 Minimization Function

In (2), if the muscle torques and moment arm matrix are known, the force vector, $f^{n\times 1}$ can be calculated through a static optimization method utilizing a cost function as shown in the work of Crowninshield [7]. A cost function is used because the body's nervous system seeks to minimize which muscles should activate based on muscle moment arm lengths and maximum muscle forces attainable by each muscle to create an external muscle torque at a joint. This cost function is expressed as

Minimize $$u(\mathbf{f}) = \sum_{i=1}^{n} (c_i \mathbf{f}_i)^r \quad (15)$$

Subject to $$\begin{cases} \tau_{MUSCLES} = \mathbf{A}(\theta)\mathbf{f} \\ 0 \le \mathrm{f}_i \le \mathrm{f}_{MAX_i} (i = 1,...,n) \end{cases}$$

where $u(f)$ is a cost function; c_i's are the weighting factors, ; r is an integer number; f_i is the muscle force for the i-th muscle; and f_{MAX_i} is the maximum muscle force for the i-th muscle. The maximum muscle forces are given according to [19] and are found in Table 1. The cost function will find a minimized solution for the muscle forces according to the "Subject to" parameters. With an accurate $\mathbf{A}(\theta)$ matrix, we are able to control both mono-articular and bi-articular muscles by combining multiple actuator forces. For the purposes of this paper, the value of r = 2 but it should be noted that there are studies using other possible values and choices of weighting factors [7], [3], [9].

For the cost function, the weighting factors c_i's will be defined as

$$c_i = \frac{1}{PCSA_i} \quad (16)$$

where $PCSA_i$ is the physiological cross sectional areas (PCSA), and $PCSA_i = \mathrm{f}_{\mathrm{MAX}_i} / \sigma_{muscle}$ where σ_{muscle} is the specific muscle strength. In this paper, σ_{muscle} = 31.39 N/cm^2 and is given according to [31].

There are arguments and criticisms however regarding the neurological background of this method and limitations of this approach. There are additional

proposed solutions to this problem such as muscle synergy and various other methods [18], [20], [25]. One argument in particular for this method could be that there is a potential limitation of a minimization function because it cannot take into account co-contraction of the muscles for increasing stiffness. However, the effectiveness of this method for predicting stereotypical muscle performance has been reported in many papers [2], [8], [15], and [29]

CHAPTER 7

METHODS FOR MUSCLE FORCE CONTROL

7.1 Iterative Method to obtain Muscle / Actuator Forces

For the purposes of exercise and this paper, attention will be focused on direct methods of control of one of the nine muscle groups and with a desired muscle profile. In an ideal case, if a person could individually specify each of the muscle forces and the position trajectory, one could directly solve for the actuator torques that would yield the muscle forces within the desired muscle profile. A person however cannot control each distinct muscle and can only control muscle torques so a process of iteration is necessary to determine which actuator torques, using the optimization function, yield the desired muscle force profile.

In order to provide a better explanation of how muscle forces are a nonlinear function, we show a constant muscle torque and the muscle forces realized through this. For this example, we are using the moment arm of the Rectus Femoris muscle (f_5) throughout its range of motion in Fig. 12 below:

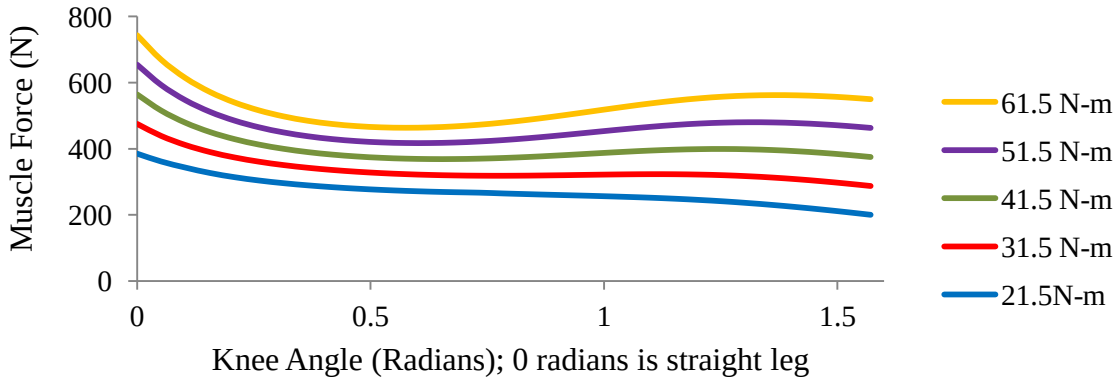

Figure 12. Five Constant Joint Muscle Torques and their corresponding muscles when factoring in nonlinear moment arm

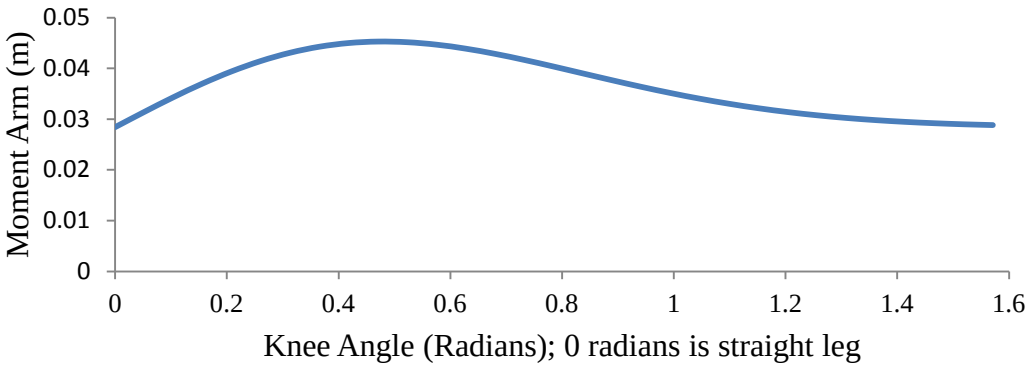

Figure 13. Moment arm of Rectus Femoris Muscle (f_5)

From Fig. 12, it is shown that a straight-line joint muscle torque will not directly control a muscle force. This is because the moment arms of each muscle change as a function of angle. An example of the rectus femoris moment arm is shown in Fig. 13. If the subject wants to be able to directly isolate or control muscles directly, then a method besides constant muscle torque is necessary. Using a direct method, it is found that a constant muscle force will not produce a constant muscle torque and is shown in Fig. 14.

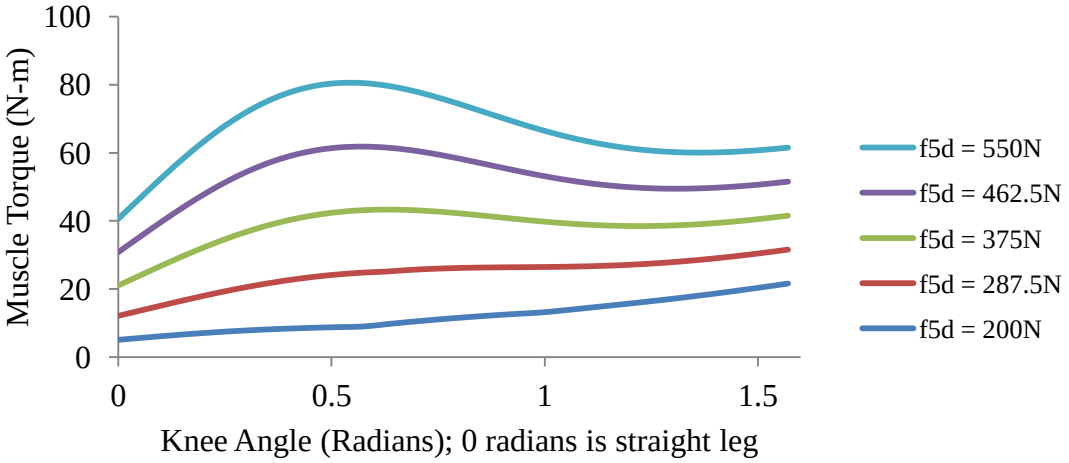

Figure 14. Five Constant Muscle Forces do not produce constant Muscle Torques

The process of finding the actuator torques to create a desired muscle force has also been investigated by Ueda but by using an analytical method instead of an iterative method for the muscles of the upper body [28]. Potential further research could include obtaining an analytical method for the lower body.

As stated, the muscle forces cannot be solved for directly and must use a method (iterative, analytical, etc.) to calculate for them. Below, is a graphic interpretation of the MATLAB iterative method in Fig. 15.

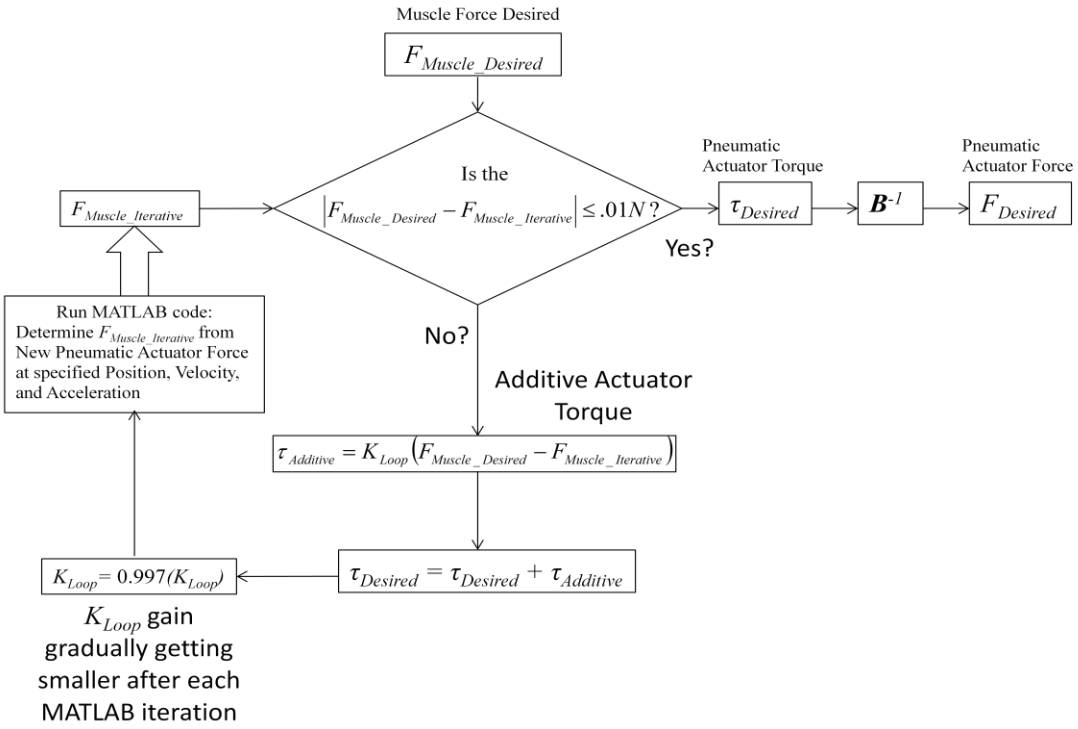

Figure 15. Iterative Method in Graphic Programming Tree Form

To better understand the iterative method, Fig. 14 describes a Desired Muscle Force is the input for the system, and uses the dynamic model of the musculoskeletal structure to determine what the Muscle Torque is needed as a function of the user's limb

velocity, gravity, and imposed torques from actuators. The system will then use the minimization function to determine what the muscle force would be for this muscle torque at the given joint angle. If the output force ($F_{Muscle\_Iterative}$) is within the threshold of being close to the Desired Muscle Force, the Actuator torque is then stored and used in the closed-loop control. If the output force is not within the threshold, the system changes the actuator torque and runs the iterative method again until it zeros in on the correct actuator torque to create the desired muscle force. When using the experimental setup in a later section, the desired force will be known as F_{5d}, or the Desired Force on the 5th Muscle Group (Rectus Femoris). The actual force coming back from the force sensor will be known as F_K, or force of the actuator on the knee joint.

Fig. 16 below highlights the complexity of the system due to even at a constant muscle force desired, the actuator torque to achieve that muscle force profile changes due to changing muscle moment arm lengths. This example removes the change of actuator torques due to gravity to isolate the change strictly due to moment arm changes.

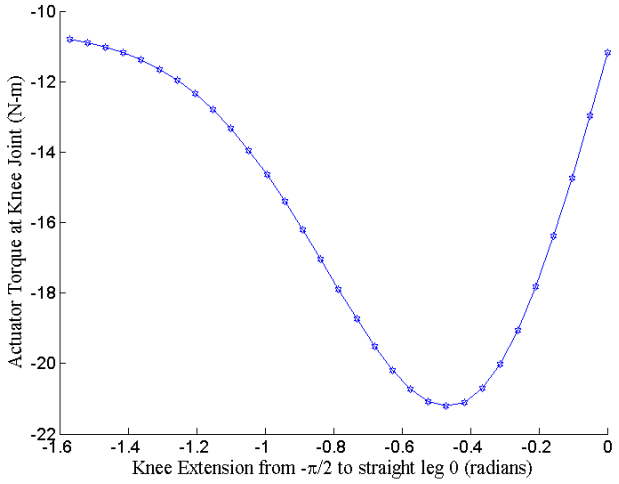

Figure 16. Actuator Torque changing due to Moment Arm in Zero Gravity for Constant 100N Muscle Force on Rectus Femoris vs. Angle

In Fig. 17, an example desired isometric muscle force profile curve is shown for the Rectus Femoris muscle as the knee moves from –π/2 radians to 0 radians (Knee Extension Exercise). From this muscle profile curve the resultant pneumatic actuator torques were calculated using an iterative method in MATLAB. The actuator torque values correspond to the muscle forces throughout the range of motion. These actuator forces are plotted in Fig. 17 through the same range of motion of Fig. 16.

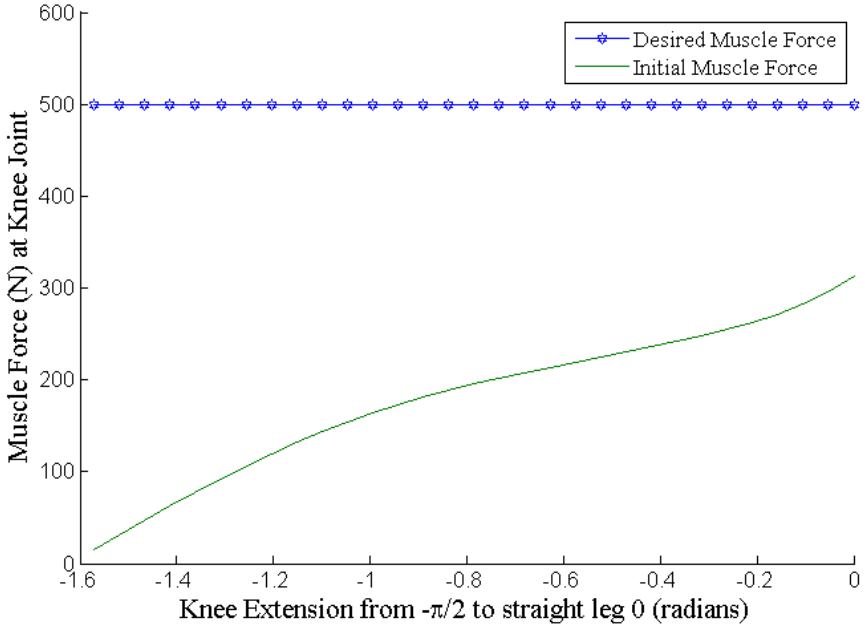

Figure 17. (Rectus Femoris) Isometric desired muscle force profile curve (pneumatic actuators + gravity) and Initial muscle force profile curve (gravity) vs. knee extension angle

The actuator torques were then multiplied by the inverse $\mathbf{B}(\theta)$ moment arm matrix to yield the actuator forces needed to obtain the desired muscle force curve. Since $\mathbf{B}(\theta)^{3\times3}$ is invertible, it is unnecessary to use a minimization function to obtain the forces involved. The force vector $\mathbf{F}^{3\times1}$ can be instead solved directly. As stated in Chapter 3.2,

since we are using only one actuator at the knee to control the Muscle Force in this experiment (with an implicit force from a hip actuator to keep hip angle constant), (3) will turn into:

$$\boldsymbol{\tau}_{\text{ACTUATOR}} = \begin{bmatrix} 0 \\ \tau_K \\ 0 \end{bmatrix} = \mathbf{B}(\theta)^{3\times 3} \begin{bmatrix} 0 \\ F_K \\ 0 \end{bmatrix} \tag{17}$$

The matrix $\mathbf{B}(\theta)$ is created by the angle of each joint. To be able to obtain the angle of the limb, a conversion is made using displacement/position data coming from the pneumatic cylinder. An equation for this conversion was derived using the parameters defined in Fig. 8. The muscle force profile curve shown in Fig. 5 is used to create the Actuator Force Curve in Fig. 18 shown below.

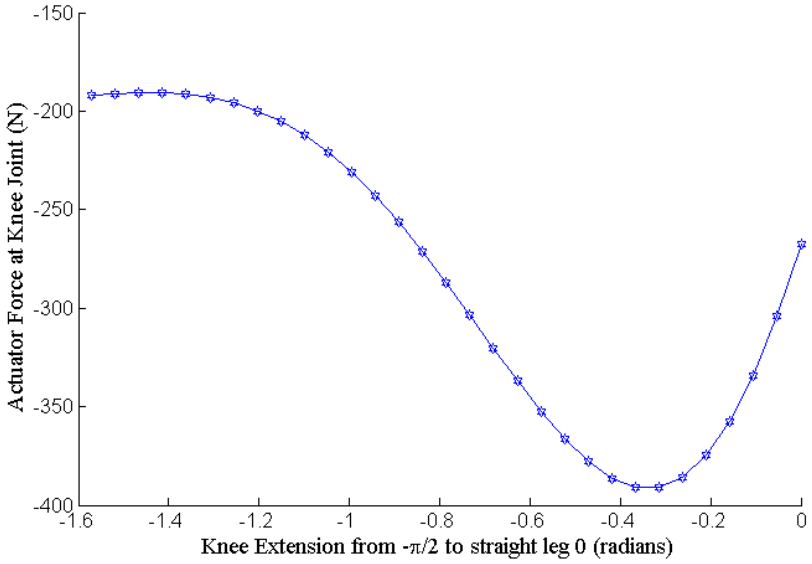

Figure 18. Desired Pneumatic Actuator Forces to produce Desired Muscle Forces vs. Knee Extension Angle

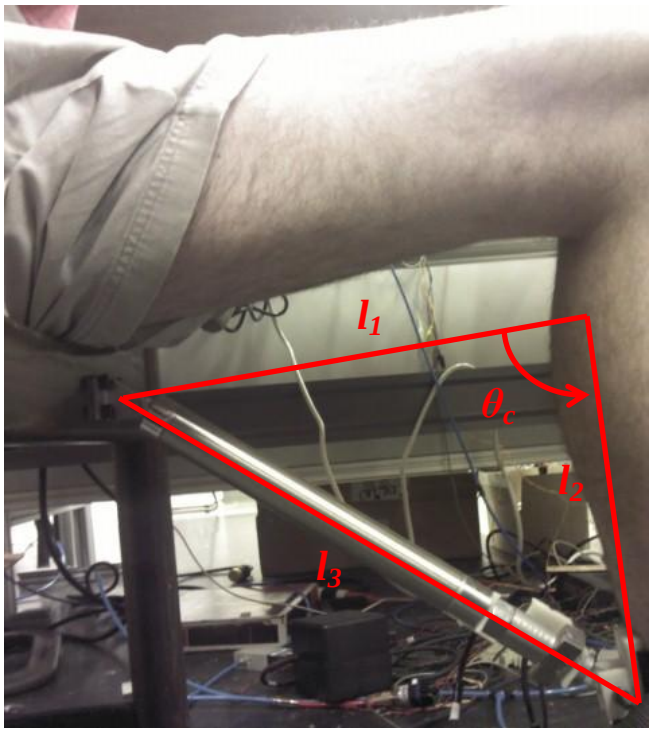

Figure 19. Calculating for Angle of Knee from Actuator Position and Moment Arm from Pneumatic Actuator to Pivot Point of Knee

For the knee joint, the relationship between X (displacement of pneumatic cylinder) and knee angle can be obtained by applying the Law of Cosines shown below and the triangle formed will be related to Fig. 19:

Law of Cosines:
$$X = -l_3 + \sqrt{l_1^{\,2} + l_2^{\,2} - 2l_1 l_2 \cos(\theta_C)} \tag{18}$$

$$\theta_C = \cos^{-1}\left(\frac{(l_3 + X)^2 - l_1^{\,2} - l_2^{\,2}}{-2l_1 l_2}\right)$$

$$\dot{X} = \frac{2l_1 l_2 \sin(\theta_K)\dot{\theta}_C}{2(l_1^{\,2} + l_2^{\,2} - 2l_1 l_2 \cos(\theta_C)^{1/2}}$$

$$\dot{\theta}_C = \frac{-1}{\sqrt{1 - \left(\frac{(l_3 + X)^2 - l_1^{\,2} - l_2^{\,2}}{-2l_1 l_2}\right)^2}}$$

where l_3 is length of cylinder at fully retracted length, l_1 and l_2 are the lengths as a function of the thigh and shank respectively; and θ_C has a range of $\pi/2$ to $3\pi/4$. θ_C is related to the actual angle of the knee through the following relationship:

$$\theta_C = (\pi + \theta_K)$$

Similar derivations are used for the following Hip and Ankle Joints as well. To determine the moment arm extending between the knee joint "pivot" point and the pneumatic cylinder, the equation is also determine from the Law of Cosines as shown below:

$$\mathbf{B}(\theta_K) = l_2 \sin\left(\cos^{-1}\left(\frac{{l_2}^2 + (l_3 + X)^2 - {l_1}^2}{2l_2(l_3 + X)}\right)\right) \tag{19}$$

7.2 Implementing Iterative Method using LabVIEW

In the previous section, it was discovered how to obtain the muscle force/s desired by varying the forces produced by the pneumatic actuator/s. The next step is controlling the muscle forces at any given joint angle.

In our setup, we use a force feedback closed-loop control with a Proportional-Integral (PI) controller. The LabVIEW system involves a "while" loop that takes in the kinematics of the subject's leg positions and velocities and uses these to run the iterative MATLAB loop stated in the previous section. This determines what actuator force to send to the controller based upon the desired muscle force profile. The MATLAB program works by specifying a muscle profile curve for a particular muscle and determining the actuator forces needed for either mono-articular or bi-articular muscles.

This reference actuator force is then put into the force feedback controller utilizing a PI control and seeks to eliminate the error between the reference actuator force and the actuator reference force from the force sensor. This then ends the "while" loop and starts at the beginning of the loop again.

Since the reference actuator force will change every while loop cycle due to the position and velocity change of the subject's leg, the iterative MATLAB method must be calculated in the while loop in the specified time allotted to having the while loop run on time. The MATLAB code must go through its iterations each while cycle because we are not solving for the minimization function using "quadprog" (MATLAB function) one time. We are iterating once using quadprog, checking how far away the desired muscle force is from the actual muscle force calculated and changing the actuator torque and running another iteration of quadprog. This is effectively solving for the inverse problem of the minimization function. The MATLAB code is also capable of changing based upon the user's acceleration but as shown below in the Experimental Validation section, the user is instructed to keep a constant velocity. When measured, the accelerations are small and the effect on the overall Actuator Force needed from the Dynamic Model of the Musculoskeletal Structure is negligible.

However, to save on computational time, a state force bank of different velocities is used to calculated multiple actuator force vs. knee angle curves before the LabVIEW while loop. Each of these curves are fitted to a 4th order polynomial as a function of the knee angle. The LabVIEW code then does not need to calculate the entire MATLAB code in real-time but instead only needs to take in the velocity data of the knee joint, determine which pre-computed velocity from the force bank it is closest to, and use that

selected polynomial to then multiply it by the knee angle to determine the desired actuator force. The size of the force bank for different velocities can be as large as desired. An example of the state force bank is shown in Fig. 20.

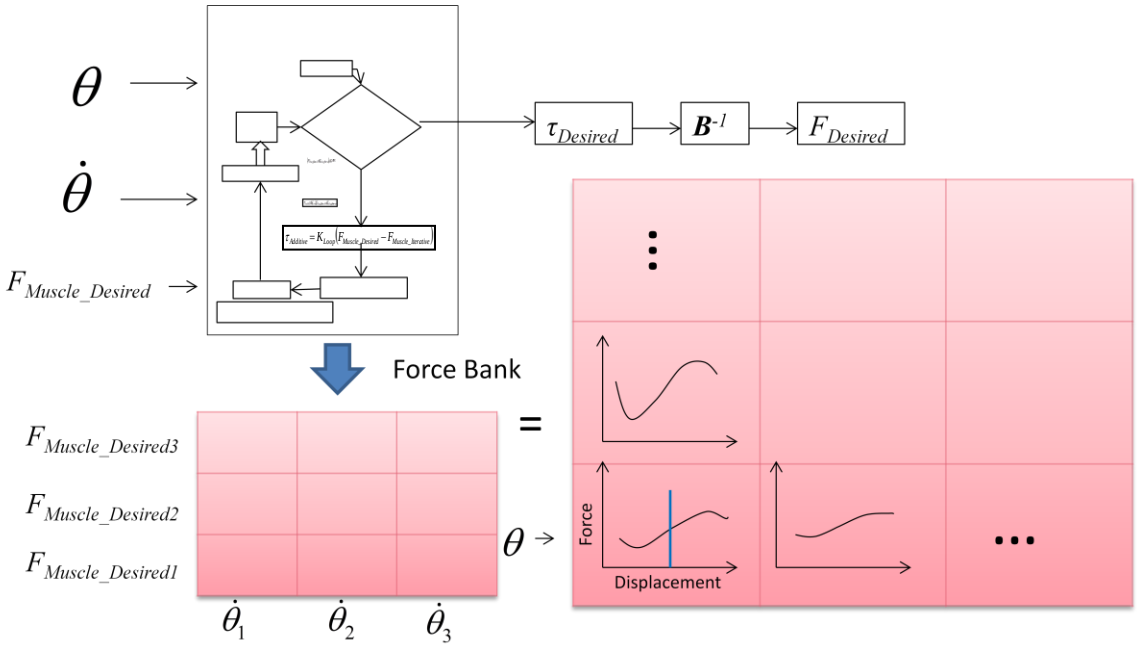

Figure 20. The iterative MATLAB method is run multiple times for various different muscle force profiles and different velocities and the terms are stored in a matrix of force-displacement curve in the form of a 4th order polynomial. All the LabVIEW program needs to do is input the velocity, knee position, and force profile desired at the moment and the output is then the desired force for the closed-loop controller to track

CHAPTER 8

HARDWARE AND EXPERIMENTAL SETUP

The understanding of how to control the forces produced by muscles for the purpose of exercise is key towards the feasibility of having humans spend longer amounts of time in a microgravity environment. The knowledge of identifying and controlling muscle forces is useful to help mitigate the negative effects of bone loss and/or muscle atrophy due to osteoporosis, inactivity, etc. on Earth as well as keeping those venturing into the depths of space in the physically fit conditions necessary for successful missions.

8.1 Setup Equipment Used

An experimental model was built to test how well the proposed actuator control method will function with real components. The exoskeleton was initially created in the computer-modeling program SolidWorks to show what the testing apparatus would potentially look like. The actual exoskeleton modeled after the SolidWorks model is shown in Fig. 25. The experiment uses a Bimba pneumatic cylinder (097-DP) shown in Fig. 21, a force sensor (Omega LCM 703-50) shown in Fig. 21, Polhemus Fastrak motion tracker for position sensing shown in Fig. 22, Festo (MPYE 05-M5-010-B) proportional valves shown in Fig. 23, Wika (Model A-10) pressure transmitter shown in Fig. 23, and National Instruments data acquisition system (NI-USB-6229) and the circuit designs for the experiment shown in Fig. 24.

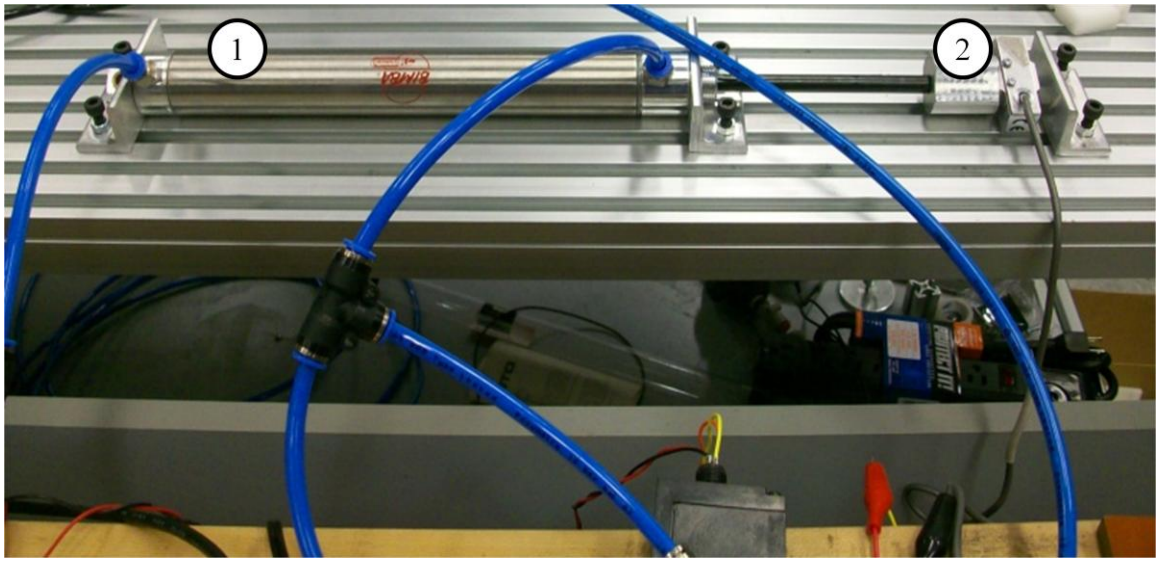

Figure 21. 1.) Bimba Actuator and 2.) Force Sensor

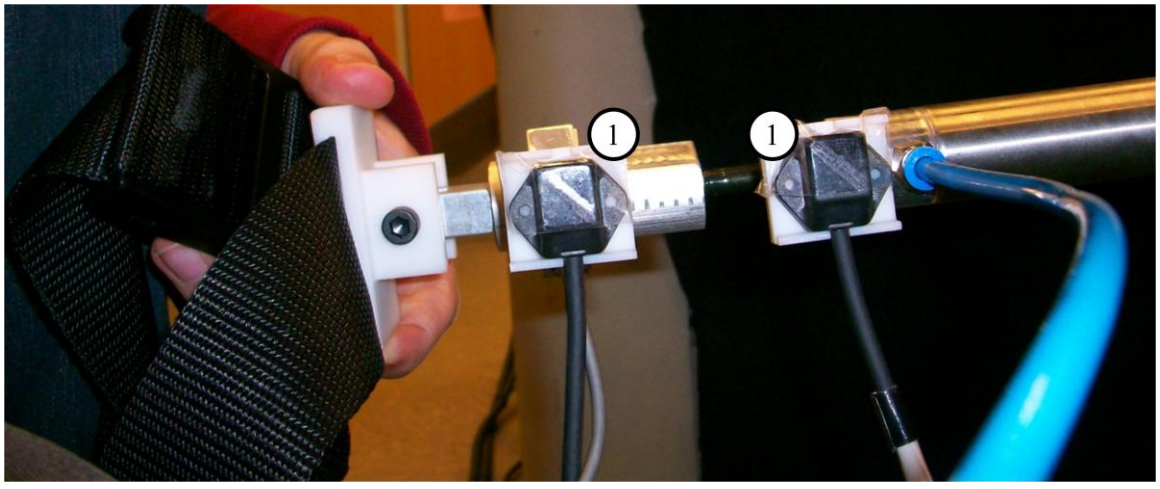

Figure 22. 1.) Polhemus Magnetic Position Sensors

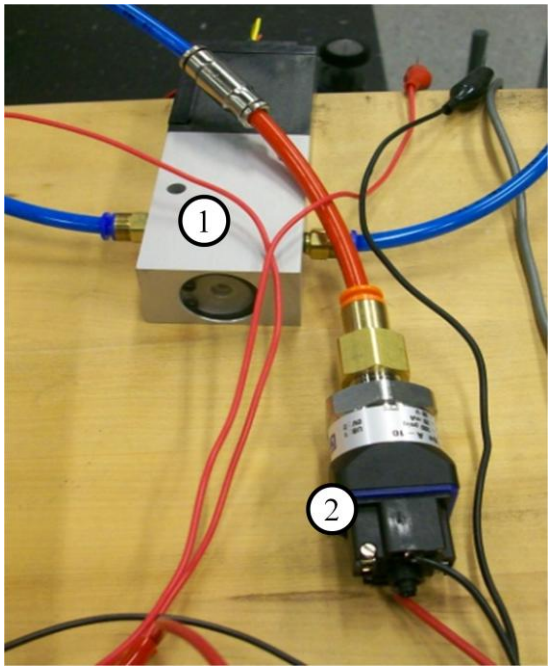

Figure 23. 1.) Proportional Valve and 2.) Pressure Sensor

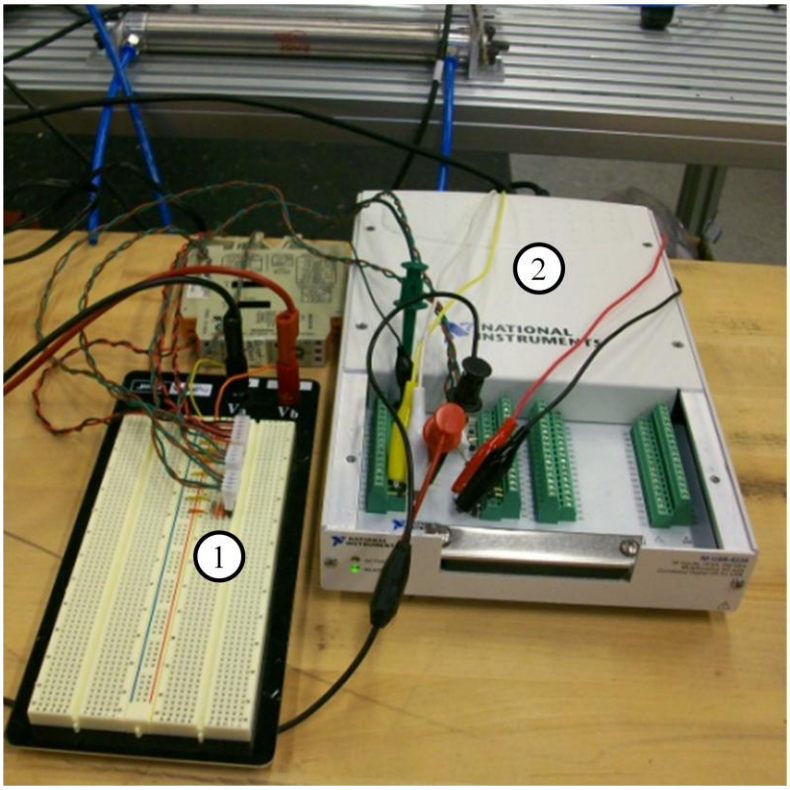

Figure 24. 1.) Wiring Design and 2.) National Instruments Data Acquisition System

8.2 EMG Tests for Iterative Method Validation

To validate the effectiveness of the current LabVIEW program, we ran nine different muscle force profiles experiments on the Rectus Femoris Muscle (f_5) for three different subjects/experimenters. The experiment involved subjecting the subject to these nine different muscle force profiles and plotting the EMG signals that resulted from the forces imposed on the leg due to gravity and the actuator. Table 4 below shows the desired muscle force profiles used for the experiment throughout the range of motion of the knee. The range of forces was chosen based upon the hardware limitations of the system for the maximum force and a minimum force so that through the range of motion of the actuator, the force signal would always be a compressive force that wants to retract the piston into the cylinder when accounting for gravity effects on the muscles.

Table 4

DESIRED MUSCLE FORCE PROFILE SETS

SET:	DESIRED MUSCLE FORCE PROFILE FOR f_{5d} (NEWTONS):
1	200
2	287.5
3	375
4	462.5
5	550
6	$200 + 300\left(\frac{\theta_K + \pi/2}{\pi/4}\right)$
7	$200 + 600\left(\frac{\theta_K + \pi/2}{\pi/4}\right)$
8	$650 - 600\left(\frac{\theta_K + \pi/2}{\pi/4}\right)$
9	$650 - 300\left(\frac{\theta_K + \pi/2}{\pi/4}\right)$

For all of experiments the subject was told to try to maintain a constant slow velocity and to keep the hip and ankle angles constant. Each experiment was run 10 times moving from $^{-\pi}/_{2}$ radians (knee bent at 90 degree angle) to $^{-\pi}/_{4}$ radians of the knee. The EMG values obtained are normalized to their maximum voluntary contraction. The velocity is also low enough for the concentric muscle exercise (< 45º-rad^{-1}) that the EMG results are negligibly affected by the knee velocity. The effects on the EMG signal are not negligible for higher velocities however and would need to be normalized to account for it [14], [30]. The whole setup is shown in Fig. 25 and the EMG electrodes attached to the leg to obtain the measurements from the rectus femoris muscle is shown below in Fig. 26.

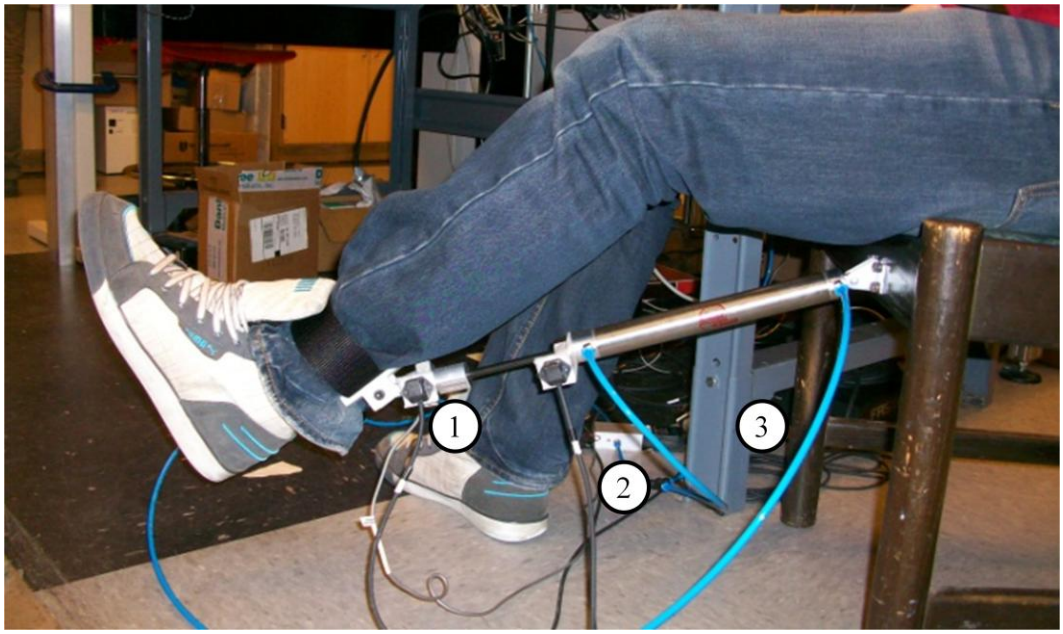

Figure 25. Physical Prototype: In Figure, 1.) Position Sensors, 2.) Proportional Valves, 3.) Pressure Sensors behind metal table leg

Figure 26. 1.) EMG Electrodes attached to leg to measure rectus femoris (f_5) muscle

CHAPTER 9

VALIDATION OF ITERATIVE METHOD FROM EMG SIGNALS

9.1 EMG experiments with different muscle force profiles

The results for the Constant Force Profiles for the three subjects are found in Fig. 27 through Fig. 30. Fig. 31 shows two different positive sloping trends and that the EMG values reflect this change with different slopes for their fitted trend lines. Fig. 32 shows how the system will only respond and move when a specified muscle force has been reach, as measured by EMG. The system will then respond by changing the desired actuator force to the controller to keep the muscle force constant in this example.

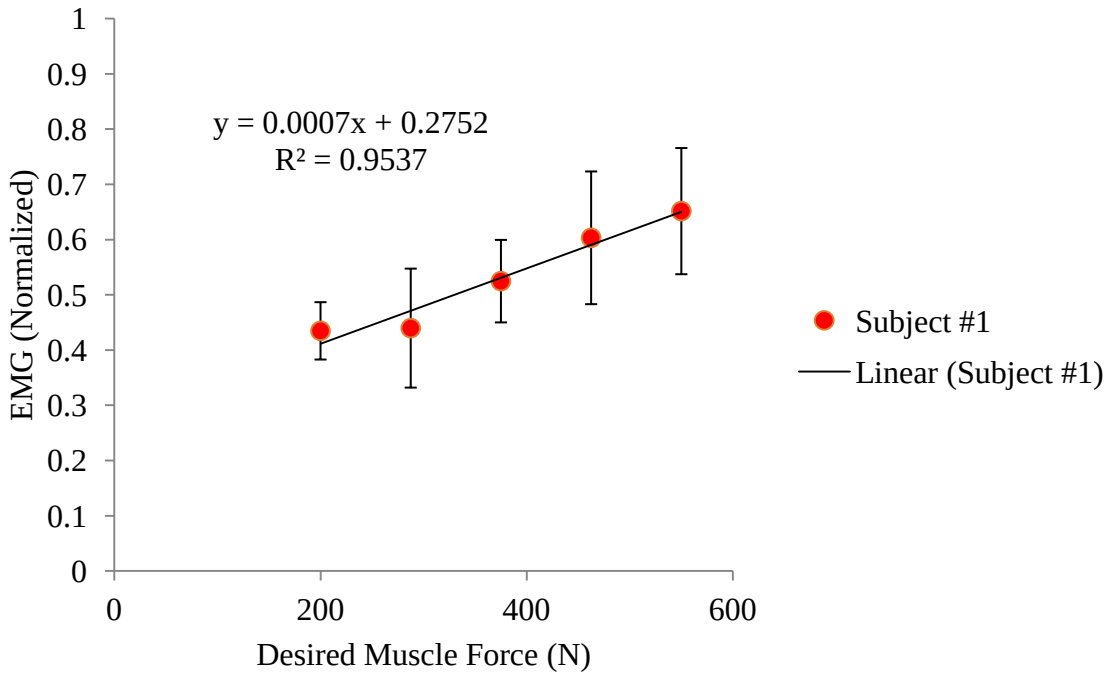

Figure 27. Subject #1: Normalized EMG Signals for specified muscle force profiles, Black Error Bar indicates ± standard deviation

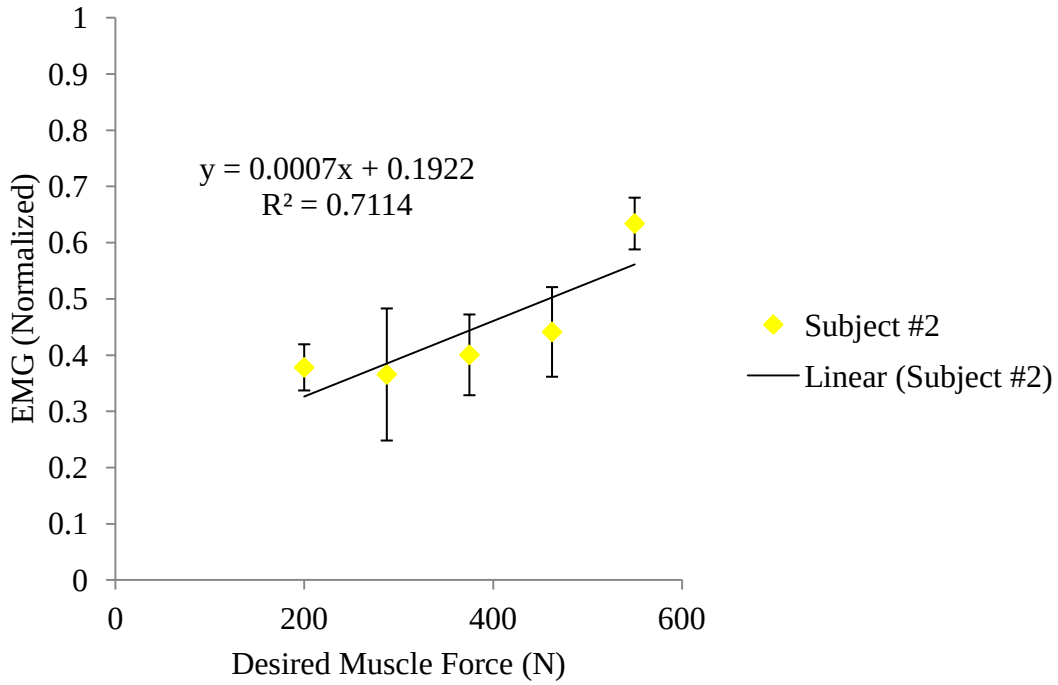

Figure 28. Subject #2: Normalized EMG Signals for specified muscle force profiles, Black Error Bar indicates ± standard deviation

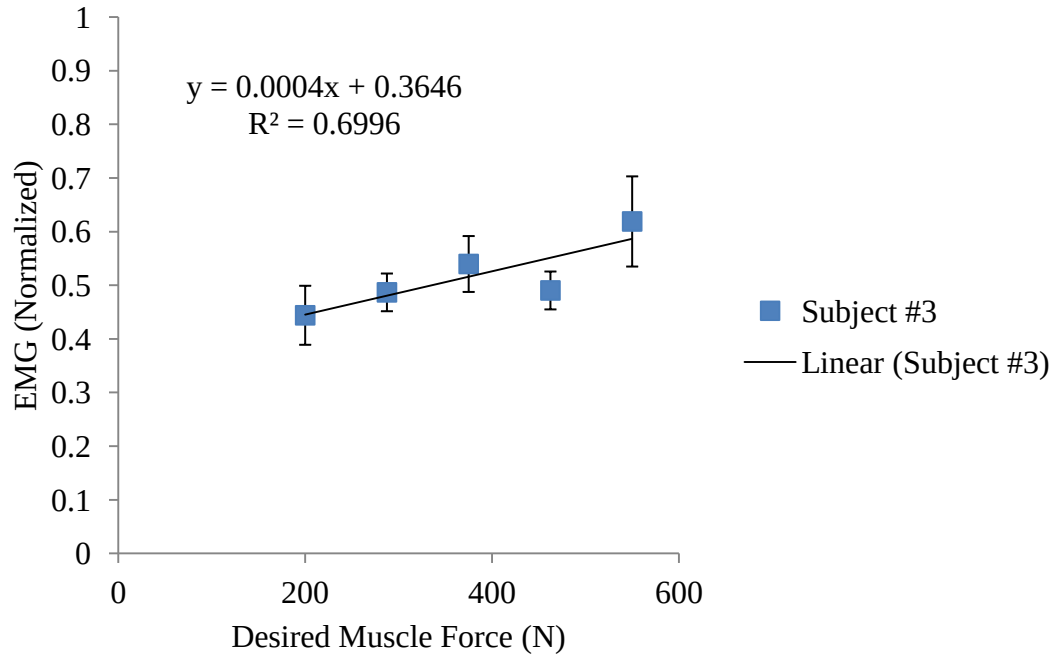

Figure 29. Subject #3: Normalized EMG Signals for specified muscle force profiles, Black Error Bar indicates ± standard deviation

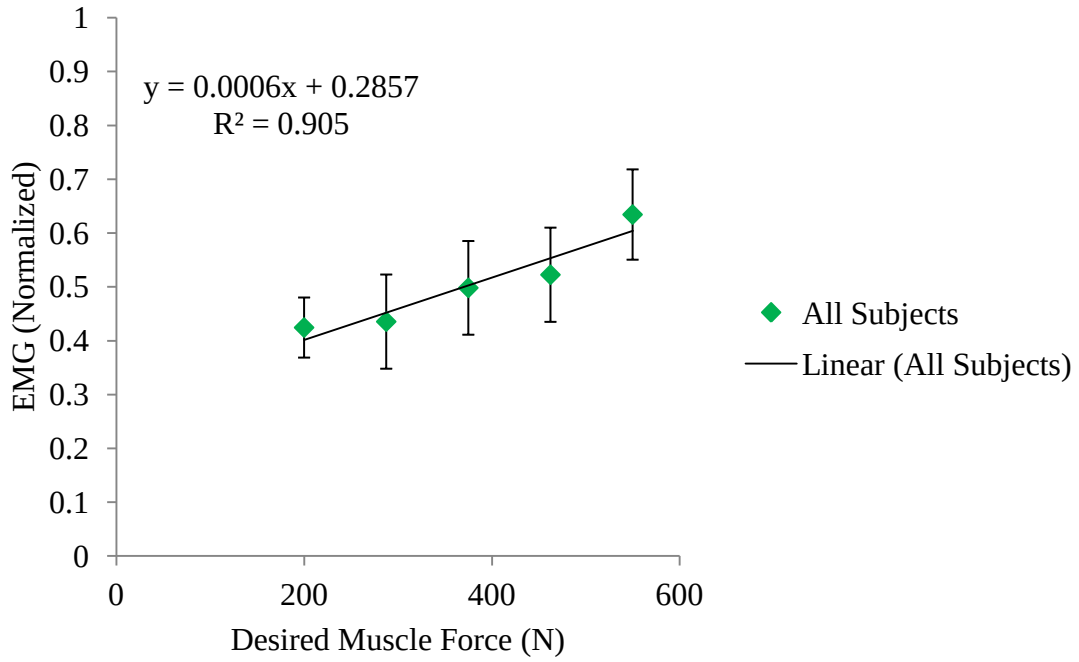

Figure 30. Normalized EMG Signals for all Subjects for specified muscle force profiles, Black Error Bar indicates ± standard deviation

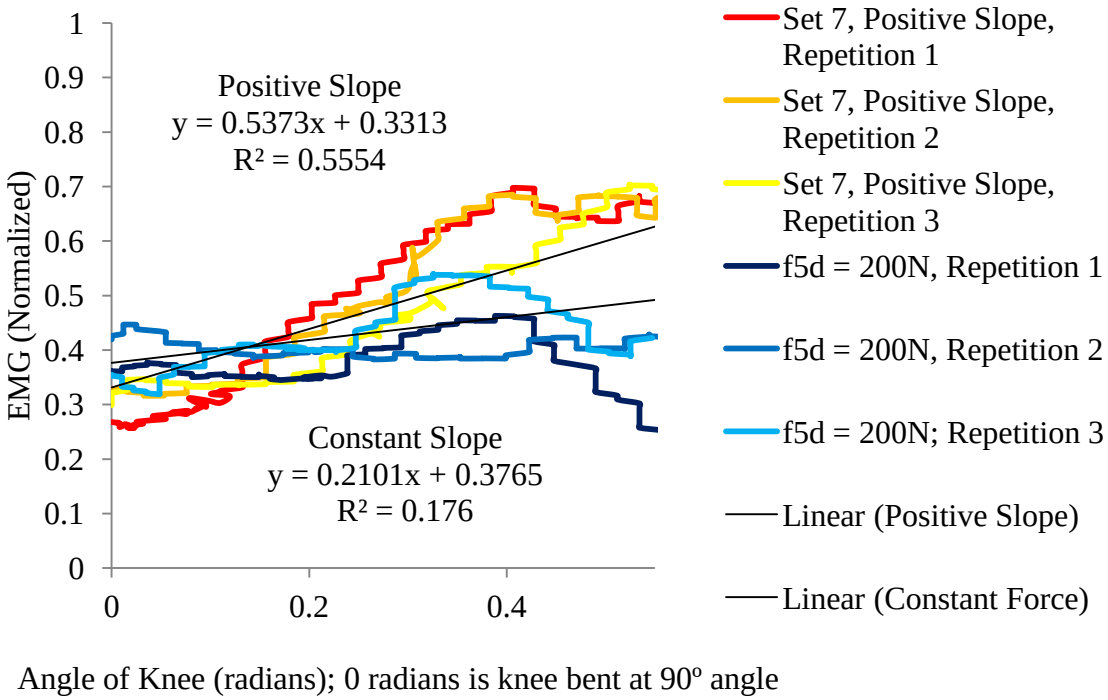

Figure 31. Normalized EMG signals for Subject #1, positive sloping muscle force profile over angle traveled, 0 radians denotes the knee is bent at a 90º angle moving towards straight leg

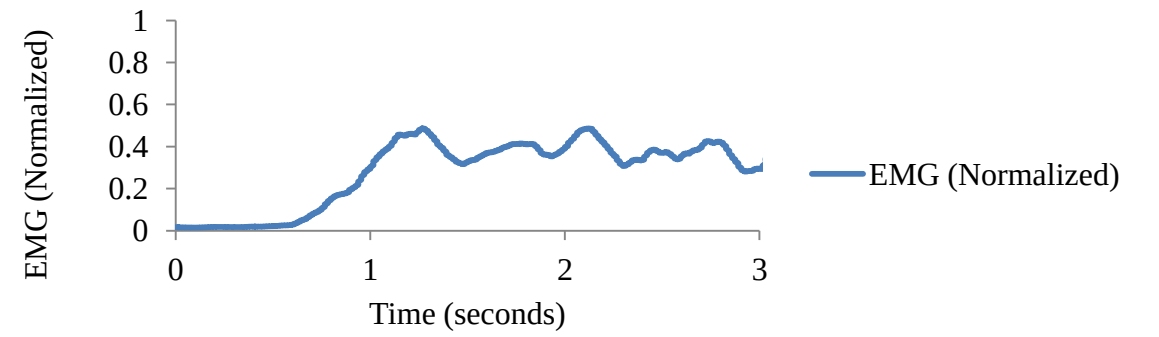

a.) Normalized EMG vs. Time

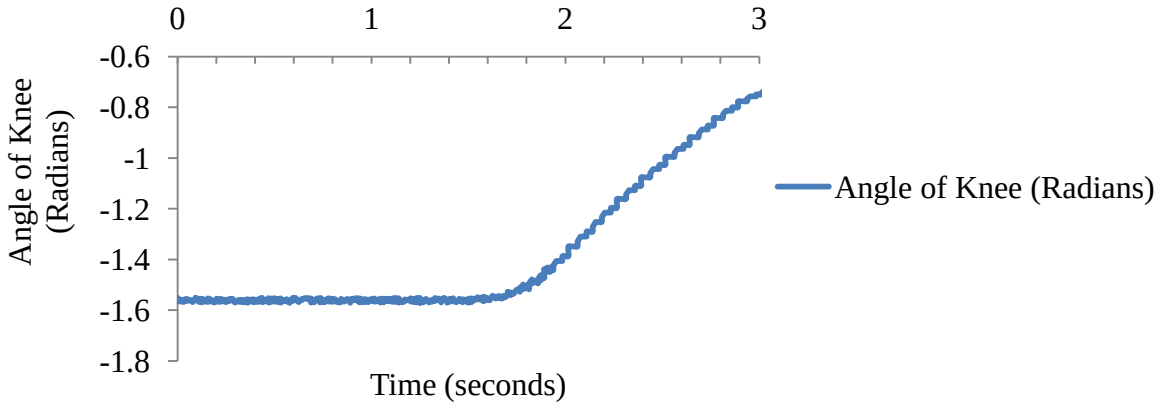

b.) Angle of Knee Joint vs. Time

Figure 32. a.) EMG vs. Time and b.) Angle vs. Time. System does not start moving until a desired EMG signal is reached at around 1.5 seconds

From the EMG data the system shows there is a statistical significance of p = .01 (99% confidence) from a student's t distribution for a one-tailed test between two muscle sets 1 and 5 in Fig. 30 on the leg to validate the force feedback controller approach. There is also a value of p = (86% confidence) and p = .06 (94% confidence) for the difference between muscle set 1 and 3 and muscle set 3 to 5 respectively.

A benchmark was created to show that there was a difference between direct control of the muscle forces through the iterative method (this research) vs. an indirect control of only controlling the joint muscle torques (discussed in Chapter 7, Section 1).

The benchmark was created by choosing one of the muscle profiles from Table 4 and comparing that to the first muscle torque value created by the iterative method. This is meant to show that both desired forces sent to the LabVIEW controller would be starting from the same point initial actual force. From there, the two force profiles sent to the controller were calculated, one through the direct method and one through the indirect method. Each test was repeated for 10 repetitions of the knee movement, a resting period, and then the same test again. The averaged results are shown in Fig. 33 below.

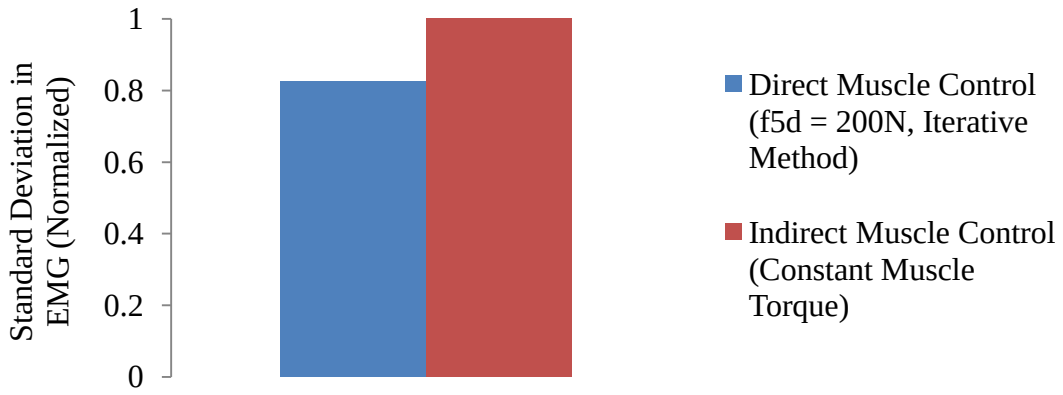

Figure 33. Direct Muscle Control (Iterative Method) vs. Indirect Muscle Control (Constant Muscle Torque); The Direct Muscle Control has 18% lower standard deviation in the EMG signal versus the Indirect Muscle Control

When the standard deviations in the EMG signals were normalized to each other, the results above were found to lower the standard deviation in the EMG signal by 18% using the method of direct control of muscles using the iterative method. This shows promise towards of the validity of this method for controlling the muscles forces directly through the iterative method versus indirectly through joint muscle torque control.

From these experimental results of a higher standard deviation in the indirect versus the direct method of muscle force control, it is useful to find the theoretical limits

of the approach. Fig. 34 below is a subset of Fig. 12 that shows plotting a constant muscle force versus plotting a constant muscle torque and the resulting muscle force that comes from it. Fig. 34 shows that for a range of knee motion that there is a standard deviation from the mean muscle force value for the indirect approach versus the constant direct muscle force approach. This states for a perfectly modeled system with perfect sensor readings (EMG) that the direct muscle approach should yield zero standard deviation in the signal while the indirect approach would yield the standard deviation from the average muscle force values over the given range of motion. Further research is necessary to adjust the LabVIEW code, MATLAB code, modeling approach, and consistency of experimental setup to obtain tighter tolerances of standard deviations in EMG data and higher resolution to realize smaller changes in muscle forces.

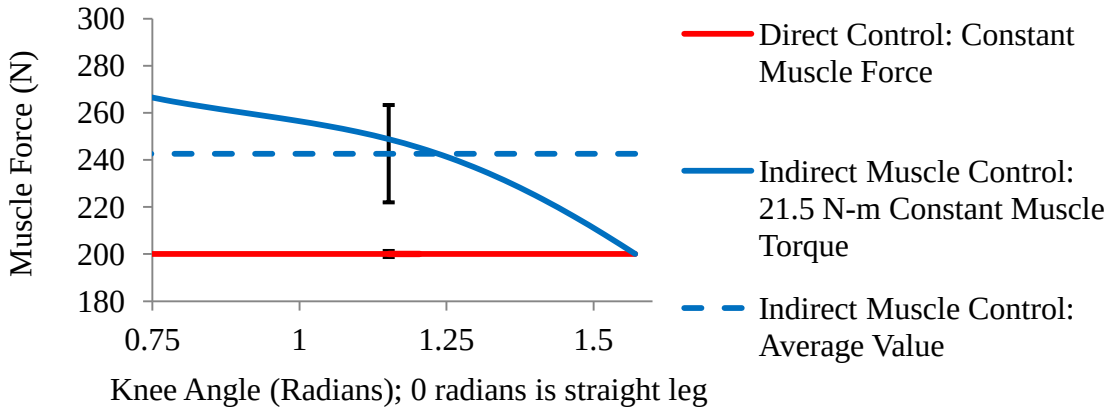

Figure 34. Direct Muscle Control (Iterative Method) vs. Indirect Muscle Control (Constant Muscle Torque); Direct Control should always have a lower standard deviation than Indirect Control

9.2 Discussion

From the results gathered, it is shown that it is possible to control the muscle force of the leg (from measuring the EMG signals) by changing the actuator forces imposed on

the leg through its range of motion. This shows that it is possible to have direct control over specified muscles forces and this would be a better source of control over exercising specific muscles versus an indirect approach of just controlling muscle torques.

Regarding the positive and negative sloping force curves subjected to the subjects, only for Subject 1 was there a difference between the two slopes of forces. It is not known what type of muscle activation profile you should have for a linear increase in force but a linear slope is used for now. The results from Subjects 2 and 3 for the positive and negative sloping force curves were not significant results.

Using the current control technique of a active quasi-dynamic Force-Feedback is able to track and realize a desired muscle force curve due to a human's low to moderate speeds (< 0.5 Hz or <.15 m/s) during exercise. If system is to be used for quicker movements (such as running), the system might not be able to create desired force quick enough for the user (hardware issue) or the actual force from sensors lags desired force signal by too much (controls issue). From a controls standpoint, a new technique would be necessary to compensate for the higher velocity potentially through methods such as more accurate plants of a inverse plant model, a tracking control with feedback and feed-forward design, or a state-machine approach with various difference mechanical impedance levels throughout the range of motion to approximate the desired muscle force profile curve.

From these results, we have found statistical significance between two of the constant muscle force profile sets imposed against the subjects. It was also found that there is statistical significance between a direct versus an indirect method of controlling the muscle forces. It should also be noted that to create the indirect method, the only

torques used to generate the force to the LabVIEW controller was force from the knee. Hip torque was not included and due to the test muscle being bi-articular, the hip could have played a part in why the constant torque value was higher. This could be considered as another un-modeled parameter in the indirect method of controlling forces and just looking at knee torque to control a muscle without regards to being bi-articular or not.

When obtaining results, it was a learning experience to see how others would utilize the lab setup when trying to maintaining a constant velocity and keeping the hip angle constant. Sources of error in the EMG signals could result from but are not limited to: low pass filter frequency needs to be lowered, this would create a smoother but delayed signal; constant placement of the subject sitting in the chair to operate the device, potentially a constraining device to keep the hip at a constant angle is needed; the magnetic position sensor being calibrated correctly for each subject involved and staying lined up in the same plane of movement the entire time; determining when a subject is fatigued after doing too many exercise sets. The data could be skewed by this after a while; determining better method of muscle normalization for different subjects to compare apples to apples when comparing EMG data from various subjects for the same desired muscle forces; and modifying LabVIEW code to reduce chatter in the force control tracking of the desired actuator force signal.

These different sources of error make it more difficult to differentiate between the EMG signals of various muscle profile sets, especially as the sets become closer to each other in terms of magnitude. Elimination of lessening of these errors can lead to better results and potentially more statistical significance in the data obtained.

CHAPTER 10

CONCLUSIONS AND FUTURE WORK

It has been determined that muscle forces cannot be controlled directly and can only be controlled indirectly through an external force such as a pneumatic actuation. To indirectly control this force, an iterative method was devised to solve for the inverse of the minimization problem that the nervous system accomplishes normally to determine how much a muscle should activate for a certain external torque needed at a certain moment arm of the muscle.

After this, the iterative method was used to determine various muscle force profiles to send to closed-loop force-feedback controller with PI control. The iterative method was validated by using three subjects/experimenters and imposes nine different muscle force profiles on them. It was found there is a statistical significance between desired muscle set 1 (f_{5d} = 200N) and a muscle set 3 (f_{5d} = 375N) (86% Confidence), and muscle set 3 to muscle set 5 (f_{5d} = 550N) (94% Confidence). There is also an 18% smaller standard deviation when comparing indirect muscle control to direct muscle control. This data is promising and prompts interest into further research to determine reasons of error in the EMG signals and slowly eliminating or lessening them. This could then result in a system that is able to impose more fine-tuned realization of different muscle forces of the muscles.

Potential future work can include more accurately control the EMG/muscle force by creating a more accurate $\mathbf{A}(\theta)$ matrix to use for computations; refining the iterative technique to obtain accurate actuator forces faster; expanding outside of the sagittal plane

into coronal plane movement with actuation forces for full range of motion of hip joint; extending experiment to multiple joints to check if target bi-articular muscles are appropriately controlled as assumed through the current MATLAB model; accounting for broad range values of acceleration in MATLAB iterations if effect on dynamics is not negligible; creating a wearable design versus a mounted design as of now to promote marketability and functionality, and discussions with Physiologists to determine desired muscle force profiles and efficient muscle exercises for patients.

REFERENCES

[1] Andersson, S., Soderberg, A., and Bjorklund, S., "Friction models for sliding dry, boundary and mixed lubricated contacts," Tribology International, vol. 40, no. 4, pp. 580-587, 2007.

[2] J. Biggs and K. Horch, "A three-dimensional kinematic model of the human long finger and the muscles that actuate it," Medical Engineering and Physics, vol. 21, no. 9, pp. 625–639, 1999.

[3] B. van Bolhuis and C. Gielen, "A comparison of models explaining muscle activation patterns for isometric contractions," *Biological Cybernetics*, vol. 81, no. 3, pp. 249–261, 1999.

[4] Book, W. and Ruis, D. (1981). "Control of a robotic exercise machine". In *Proc. of the Joint Automatic Control Conference*, pages WA.2A.

[5] V. J.Caiozzo, M. J. Baker, R. E. Herrick, M. Tao, and K. M. Baldwin. Effect of a spaceflight on skeletal muscle: mechanical properties and myosin isoform content of a sow muscle. *J. Appl. Physiol.* 76, 1764–1773, 1994

[6] V.A. Convertino, Exercise and its use as a countermeasure against physiological adaptation to prolonged spaceflight. Med. Sci. Sports Exerc. 28:000-000, 1996

[7] RD. Crowninshield, et al., "A physiologically based criterion of muscle force prediction in locomotion," *J. Biomechanics*, vol. 14, pp. 793–801, 1981.

[8] S. Delp, J. Loan, M. Hoy, F. Zajac, E. Topp, J. Rosen, V. Center, and P. Alto, "An interactive graphics-based model of the lower extremity to study orthopaedic surgical procedures," Biomedical Engineering, IEEETransactions on, vol. 37, no. 8, pp. 757–767, 1990.

[9] Erdemir, A., McLean, S., Herzog, W., van den Bogert, A.J., 2007. Model-based estimation of muscle forces exerted during movements. Clinical Biomechanics 22, 131–154.

[10] J. Furusho, M. Sakaguchi, N. Takesue, and K. Koyonagi, "Development of ER brake and its application to force display," *J. Intell. Mater. Syst. Struct.*, vol. 13, pp. 425–429, 2002.

[11] D. Karlsson and B. Peterson, "Towards a model for force predictions in the human shoulder," Journal of biomechanics, vol. 25, no. 2, pp.189–199, 1992.

[12] H. Kawamoto, Suwoong Lee, S. Kanbe, and Y. Sankai. Power assist method for HAL-3 using EMG-based feedback controller. *IEEE International Conference on Systems, Man and Cybernetics*, 2:1648–1653, 2003

[13] H. Kazerooni, J.-L. Racine, L. Huang, and R. Steger. On the control of the Berkeley Lower Extremity Exoskeleton (BLEEX). *IEEE International Conference on Robotics and Automation*, pages 4353–4360, April 2005.

[14] Kellis E and Baltzopoulos V., "Muscle activation differences between eccentric and concentric isokinetic exercise" *Med Sci Sports Exerc* 30: 1616–1623, 1998.

[15] W. Maurel and D. Thalmann, "A Case Study on Human Upper Limb Modeling for Dynamic Simulation," Computer Methods in Biomechanics and Biomedical Engineering, vol. 2, no. 1, pp. 65–82, 1999.

[16] E.R. Morey. Spaceflight and bone turnover: correlation with a new rat model of weightlessness. Bioscience 29:168–172. 1979

[17] E.R. Morey-Holton, RK. Hindlimb unloading of growing rats: a model for predicting skeletal changes during space flight. Bone 1998; 22 (5): 83S-8S

[18] Patriarco, A. B., Mann, R. W., Simon, S. R., and Mansour, J. M., 1981, ''An Evaluation of the Approaches of Optimization Methods in the Prediction of Muscle Forces During Human Gait,'' J. Biomech., 14, pp. 513–525.

[19] S.J. Piazza, S.L. Delp. The influence of muscles on knee flexion during the swing phase of gait. *Journal of Biomechanics* 29,723–733. 1996.

[20] Raikova, R.T., Prilutsky, B.I., 2001. Sensitivity of predicted muscle force to parameters of the optimization-based human leg model revealed by analytical and numerical analyses. J. Biomech. 34, 1243–1255.

[21] R. Riener and T. Fuhr, "Patient-driven control of FES supported standing-up: a simulation study," *IEEE Trans. Rehab. Eng.*, vol. 6, pp.113–124, June 1998.

[22] S.M. Schneider, Ww.E. Amonette, K. Blazine, J. Bentley, S.M. Lee, J.A. Loehr, A.D. Moore Jr, M. Rapley, E.R. Mulder, S.M. Smith. Training with the International Space Station interim resistive exercise device. *Med Sci Sports Exerc* 35: 1935–1945, 2003.

[23] X. Shen, and M. Goldfarb. "Simultaneous Force and Stiffness Control of a Pneumatic Actuator". Journal of Dynamic Systems, Measurement, and Control. Vol 129, 425-434 July 2007

[24] Shu, N. and Bone, G.M., "Development of a nonlinear dynamic model for a servo pneumatic positioning system," in *Mechatronics and Automation, 2005 IEEE International Conference*, vol. 1, 00. 43-48 Vol. 1, 2005

[25] Stokes, I.A.F., Gardner-Morse, M., 2001. Lumbar spinal muscle activation synergies predicted by multi-criteria cost function. Journal of Biomechanics 34, 733–740.

[26] Thayer, W. J., 1958, ‘‘Transfer Functions for Moog Servovalves,’’ *Moog Technical Bulletin 103*, East Aurora, Moog Inc., Controls Division, New York

[27] S. Trappe, D. Costill, P. Gallagher, et al. Exercise in space: human skeletal muscle after 6 months aboard the International Space Station. *J Appl Physiol.* 2009;106:1159–1168.

[28] J. Ueda, D. Ming, V. Krishnamoorthy, M. Shinohara, and T. Ogasawara. “Individual Muscle Control using an Exoskeleton Robot for Muscle Function Testing” *Transactions on Neural Systems and Rehabilitation Engineering*. Vol 18, 339-350, Aug. 2010

[29] H. Veeger, F. Van der Helm, L. Van der Woude, G. Pronk, and R. Rozendal, “Inertia and muscle contraction parameters for musculoskeletal modeling of the shoulder mechanism,” J Biomech, vol. 24, no. 7, pp.615–29, 1991.

[30] Westing, S. H., A. G. Cresswell, and A. Thorstensson. Muscle activation during maximal voluntary eccentric and concentric knee extension. Eur. J. Appl. Physiol. 62:104-108, 1991.

[31] G. Yamaguchi, *Dynamic modeling of musculoskeletal motion*. Kluwer Academic Publishers, 2001.

[32] Zhu, Y. and Barth, E.J., "Impedance control of a pneumatic actuator for contact tasks," in *2005 IEEE International Conference on Robotics and Automation, April 18, 2005 - April 22, 2005*, vol. 2005 of Proceedings - *IEEE International Conference on Robotics and Automation*, p. 987 - 992, Institute of Electrical and Electronics Engineers Inc., 2005. Compilation and indexing terms, Copyright 2010 Elsevier Inc. 20070310371365 Contact forces Impedance control Pneumatic actuation Pressure tracking Proportional spool valves